1994ApJ...421..412W

THE ASTROPHYSICAL JOURNAL, 421:412–433, 1994 February 1
© 1994. The American Astronomical Society. All rights reserved. Printed in U.S.A.

A WIDE-FIELD MULTICOLOR SURVEY FOR HIGH-REDSHIFT QUASARS, $z \geq 2.2$. III. THE LUMINOSITY FUNCTION

STEPHEN J. WARREN
European Southern Observatory, Karl-Schwarzschild-Straße 2, W-8046 Garching bei München, Germany; and
Nuclear and Astrophysics, University of Oxford[1], Keble Road, Oxford OX1 3RH, UK
E-mail: sjw@oxds02.astro.ox.ac.uk

PAUL C. HEWETT
Institute of Astronomy, University of Cambridge, Madingley Road, Cambridge, CB3 0HA, UK
E-mail: phewett@mail.ast.cam.ac.uk

AND

PATRICK S. OSMER
National Optical Astronomical Observatories[2], Box 26732, Tucson, AZ 85726[3]
E-mail: posmer@payne.mps.ohio-state.edu
Received 1993 April 8; accepted 1993 August 9

ABSTRACT

In two previous papers we presented the aims, methods, and spectroscopic results, and computed the completeness of a six-band multicolor survey for high-redshift quasars, covering an effective area of 43.0 deg^2, to $m_{or} = 20.0$. In this paper the complete sample of 86 quasars $2.2 \leq z < 4.5$ is combined with other published samples to determine the continuum and line luminosity functions, Φ_C, Φ_L, over the redshift range $2.0 \leq z < 4.5$.

The estimate of the completeness of our multicolor sample has been revised following the development of a more sophisticated treatment of the line and continuum absorption from intervening matter, and the incorporation of the effects of quasar variability. Appendices describe the new model procedures. The luminosity function calculation also accounts for the range of line strength and continuum spectral index, as well as the photometric errors. The results are presented in terms of two magnitudes, $M_{C(1216)}$ and $M_{L(1216)}$, which are logarithmic measures of the absolute continuum flux under the Lyα/N v emission line, and of the Lyα/N v line luminosity. Additionally the intrinsic distribution of continuum spectral indices α is derived. This completes the parameterization of the rest-frame UV spectral-energy distributions of the quasar population, in the four-dimensional space with axes $M_{C(1216)}$, $M_{L(1216)}$, α, z.

The nature of the evolution of the continuum luminosity function changes near the midpoint of the redshift interval, and no simple model provides a satisfactory fit over the entire redshift range $2.0 \leq z < 4.5$. For redshifts $z < 3.5$, no-evolution luminosity functions, and luminosity functions of evolving single power-law form are inadequate. The best fit is obtained with functions of the Schechter or double power-law type, in which only the bright end evolves, to brighter magnitudes at higher redshift. The evolution ceases near $z = 3.3$, with a marked decline in space density beyond.

Comparison of the number of survey quasars in the redshift range $3.5 \leq z < 4.5$ against the number expected if there is no decline beyond $z = 3.3$ shows a shortfall by a factor 6.1(6.5), for $q_0 = 0.1(0.5)$. At the 95% confidence level there is a decline in the space density of quasars $M_C < -25.6(< -24.5)$ between redshifts $z = 3.3$ and 4.0 by a factor greater than 3.1(>3.3). These limits include an allowance for the uncertainty in the estimate of the luminosity function at $z = 3.3$. Our results are very similar to those obtained by Osmer a decade ago. A similar comparison against the preliminary results of the brighter survey of Irwin et al. indicates that the amount of the decline is approximately independent of absolute magnitude, brighter than the above limits. The observed decline in the space density of quasars beyond $z = 3.3$ is compatible with a constant true space density and obscuration by dust in intervening damped Lyα systems only if the parameters of the obscuration (dust to gas ratio, etc.) are at the upper end of current observational limits. The line luminosity function at $z = 3$ and 4 is computed, to compare against the forthcoming results of the wide-field grism survey of Schmidt et al.

Subject headings: galaxies: luminosity function, mass function — quasars: general — surveys

1. INTRODUCTION

The nature of the evolution of the quasar luminosity function at high redshifts (here taken to mean the redshift range $2.2 \leq z < 4.5$) provides constraints on the growth of structure in the early universe and the formation of quasars themselves (e.g., Haehnelt & Rees 1993). The determination of the behavior of the quasar luminosity function for redshift $z > 2$, therefore, remains a question of outstanding interest. Although the first quasars with redshifts exceeding $z = 4$ were discovered some years ago (Warren et al. 1987; Schmidt, Schneider, & Gunn 1987), the completion of the major observational campaigns necessary to acquire samples of high-redshift quasars of

[1] Postal address.
[2] NOAO is operated by the Association of Universities for Research in Astronomy, Inc., under cooperative agreement with the National Science Foundation.
[3] Current address: Department of Astronomy, Ohio State University, 174 W. 18th Ave., Columbus, OH 43210.

© American Astronomical Society • Provided by the NASA Astrophysics Data System

1994ApJ...421..412W

significant size has occurred only recently (Warren, Hewett, & Osmer 1991b; Irwin, McMahon, & Hazard 1991; Schmidt, Schneider, & Gunn 1991). A detailed understanding of the data and the procedures applied to select candidate quasars is then required before the samples may be used to derive quantitative estimates of the form of the luminosity function and its evolutionary behavior. Acquiring a quantitative understanding of the data and the effectiveness of the selection procedures is a formidable undertaking, involving a similar level of complexity and effort to that required to compile the quasar samples themselves. The results of such investigations are now becoming available, and this paper presents our calculation of the quasar luminosity function for redshifts $2.0 \leq z < 4.5$.

The analysis is based on the multicolor-selected sample of 85 quasars presented in the two earlier papers of this series (Warren et al. 1991a, b, hereafter Papers I and II, respectively). The rationale of the survey described in Papers I and II was to obtain a sample of high-redshift quasars $2.2 \leq z < 4.5$, selected using precisely specified color criteria. In this way, by modeling the colors, it is possible to compute the probability that a quasar of given spectral type, brightness, and redshift would have been found, and thereby to infer the true space density. Paper I presented the aims and methods of the survey, and the results of the calculation of the sample completeness. Paper II presented the catalog of the quasars discovered in the survey, and the measurements of the apparent magnitudes, line equivalent widths (EWs), and continuum spectral indices. A precis of the contents of Papers I and II is provided in § 2.

Since the publication of Paper I we have made two improvements to the procedures employed to generate synthetic colors for a quasar of specified spectral energy distribution (SED), adopting a more detailed model for intervening absorption, and accounting for the effect on quasar colors of variability. In § 3 we review the reasons for, and the main consequences of, the refinements to the modeling procedures, and details of the models are provided in Appendices A and B. The revised detection probabilities are higher than those presented in Paper I. The quasar catalog, listing the detection probability for each quasar, is included as Appendix C. Also described there are minor changes to the quasar sample made since the publication of Paper II. These involve the addition of one quasar, bringing to 86 the total number in the complete sample, and small modifications to the relative numbers of quasars in each of the nine spectral-type classes.

Conventionally the measure of the luminosity of optically selected quasars is the absolute magnitude at a rest-frame wavelength of $\lambda = 4400$ Å, M_B. At high redshifts the extrapolation from the rest-frame wavelengths observed in the *or* passband, $\lambda \sim 1500$ Å, to $\lambda = 4400$ Å introduces large uncertainties in the derived absolute magnitudes. For this reason we have chosen to use $\lambda = 1216$ Å as the reference wavelength. This approach also allows the results of this paper to be compared more readily with results from Lyα-line-selected samples such as the those of Schmidt et al. In § 4 we provide the equations that relate the observed quantities (apparent magnitudes, line fluxes) to the continuum and emission-line absolute magnitudes.

In § 5 the calculation of the quasar luminosity function and its evolutionary behavior is presented. The analysis employs our multicolor sample and other published samples, and covers the redshift range $2.0 \leq z < 4.5$. In § 5.1 the binned estimate of the luminosity function at different redshifts is provided. This calculation confirms the existence of a decline in the space density of quasars at redshifts $z \gtrsim 3.5$, first reported by Osmer (1982). This is the main result of this paper. In § 5.2 we describe the procedures involved in the maximum-likelihood fitting of parametric models for the luminosity function. Application of the maximum-likelihood procedures to determine the range of parametric models that can be excluded, and those that remain variable, is described in § 5.3. In § 5.4 the principal conclusions of the analysis are summarized and quantitative limits set on the degree of the decline in space density at redshifts $z > 3.5$.

The results of § 5 are based on complex selection functions and large corrections for incompleteness. In § 6 we use all the known quasars in the south Galactic pole (SGP) field, including several not in the complete sample, to provide lower limits to the numbers of quasars at redshifts $z = 3$ and $z = 4$, to compare against the results of § 5. In § 7 we provide predictions of the results of two other major surveys for high-redshift quasars, the wide-field $b_j ri$ survey of Irwin et al. (1991) and the grism survey of Schmidt et al. (1991). A summary of the principal conclusions of the paper is given in § 8.

Readers interested in the details of the calculation of the survey selection function, the definitions and equations employed to calculate continuum absolute magnitudes, and their relation to other parameterizations of the quasar SEDs such as emission-line luminosity will wish to address the entire paper. Those who are interested primarily in the results may want to read § 3, which discusses issues that have wide applicability for many quasar surveys, and then proceed to § 5.1, § 5.3, and § 5.4, where the main results are presented. Comparison with other surveys, in § 7, may also be of interest.

2. THE SURVEY

Two fields were surveyed using photographic plates taken with the United Kingdom Schmidt Telescope (UKST), covering a total area of 58.6 deg^2. Pairs of plates in each of six passbands, u, b_j, v, *or*, r, i, in each field were scanned by the Automated Plate Measuring facility, and catalogs of six-band photometry were compiled for every object that was detected on both of the *or* plates. Objects with extended or flawed images and objects with images merged with a neighbor on any of the plates were removed, and the catalogs were limited by brightness, to $16.00 \leq m_{or} \leq 20.00$ in the SGP field (29,815 stellar objects), and to $16.00 \leq m_{or} \leq 19.82$ ($15.86 \leq m_{or} \leq 19.68$ after correction for Galactic reddening) in the field F401 (113,919 stellar objects). The cleaning process eliminates some stellar objects and the effective area of the survey was reduced to 45.7 deg^2.

The six broad-band magnitudes are the coordinates of each object in a six-dimensional (6-D) parameter space in which most objects, that is, normal Galactic stars, lie in an elongated clump. Outliers include quasars, rare types of star, and some galaxies that are unresolved on the plates. The sample of quasars to be used in the calculation of the luminosity function was obtained by using spectra to classify all the objects in a list of outliers, as follows. The 6-D distance of each object to its tenth nearest neighbor was used to rank all outliers. A guillotine was applied to the list, thereby selecting only the outliers farthest from the stellar locus. Objects bluer than a specified value of $m_u - m_{b_j}$ were excluded, to ensure that the sample was not dominated by quasars with redshifts $z < 2.2$, a redshift range where large samples were already in existence. Low-resolution spectra on a UKST objective-prism plate of each field were used to eliminate obvious bright stars in this list,

© American Astronomical Society • Provided by the NASA Astrophysics Data System

1994ApJ...421..412W

leaving 216 outliers (123 in the SGP, 93 in F401), of which 18 were already known to be quasars, 14 of high redshift $z \geq 2.2$.

Intermediate-resolution spectra were obtained of 179 of the remaining 198 candidates, at the Anglo-Australian Telescope and the 4 m telescope at Cerro Tololo, and revealed a further 71 high-redshift quasars. A correction to the effective area of the survey of 6% was made to account for the few high-redshift quasars remaining among the 19 unclassified outliers. This correction was established from the ranking of the 19 outliers, knowing how the proportion of quasars in the list varied by rank. In summary, the 85 high-redshift quasars $z \geq 2.2$, hereafter referred to as the complete sample, are all the quasars that satisfy the selection criteria in an effective area of 43.0 deg^2. There are 60 in the SGP and 25 in F401. The uneven split is a consequence of the much greater number of stars in F401 and the resulting reduction in efficiency of the technique. A further 29 high-redshift quasars were discovered by exploring deeper the contents of the photometric catalogs in a subjective manner. Combined with the complete sample these quasars provide a lower limit to the space density at high redshifts.

For a specified redshift and apparent magnitude, the probability that a quasar would achieve membership of the complete sample depends on the SED. The full description of the complete sample, then, comprises the distribution in the apparent magnitude versus redshift plane, and the distribution of SEDs. It follows that in computing the luminosity function one must at the same time solve for the true distribution of spectral properties that corresponds to that observed. Accordingly we divided the complete sample into nine spectral classes, defined by a grid of three ranges of the strength of the Lyα/N v emission line, and three ranges of the continuum spectral index. We computed the detection probability over the apparent magnitude and redshift ranges of the survey for each of the nine spectral classes, for both fields. These 18 selection functions were presented as contour plots in Paper I.

3. MODELING QUASAR COLORS: INTERVENING ABSORPTION AND INTRINSIC VARIABILITY

To compute the detection probability for any quasar (Paper I) we simulated the expected distribution of colors for the particular intrinsic SED to find what fraction of this distribution in the 6-D magnitude space lies beyond the selection distance threshold. The factors that cause a spread in colors that we considered in Paper I are line and continuum absorption from Lyα clouds, Galactic absorption, and the photometric errors. Subsequently, a detailed comparison between the results of the simulations presented in Paper I and the colors of the detected quasars revealed some discrepancies. These arise from two sources: first, a more detailed model for the line and continuum absorption due to Lyα clouds is required to reproduce the observed $m_u - m_{b_j}$ colors of the quasars. Second, there is an additional spread in the observed colors associated with photometric variability of the quasars over periods of years, since the plates were taken at several different epochs.

The effects of intervening absorption and variability are discussed here, and the details of the models are provided in Appendices A and B. The detection probabilities for the individual quasars given in Table 12 (Appendix C) take into account these revisions to the modeling procedures. Examples of the revised selection functions are given in Figure 2.

3.1. *Intervening Absorption*

At redshifts where optical passbands probe wavelengths below 1216 Å in the quasar rest frame the observed colors of quasars are strongly influenced by absorption from neutral hydrogen along the line of sight. The effects become even more pronounced at higher redshifts where the density of absorption lines increases and where continuum absorption from any intervening optically thick clouds modifies the intrinsic SED of the quasars at rest-frame wavelengths <912 Å to an even greater extent. In our multicolor data the effects of the intervening absorption manifest themselves particularly as an extreme spread, $\Delta m \sim 3$ mag, in the observed $m_u - m_{b_j}$ colors of the quasars in the redshift range $3.0 < z < 3.5$. The existence of strong intervening absorption reddens the observed $m_u - m_{b_j}$ colors, moving the quasars away from the locus of main-sequence stars in the multicolor space, making them more readily detectable.

To improve the match between the simulated quasar colors and the data, a more sophisticated treatment of the effects of intervening absorption has been incorporated. The refined treatment follows that of Møller & Jakobsen (1990) and is described further in Møller & Warren (1991). The absorption due to each line in the Lyman series (to L17) is now modeled explicitly, with the result that the rollover close to the Lyman limit caused by the crowding of the Lyman series is well reproduced. The continuum absorption from all the lines is now accounted for, regardless of optical depth, whereas previously only the Lyman-limit systems ($\tau > 1$) were treated. Figure 1*a* provides an illustration of the simulated quasar colors. This figure shows a ub_jv two-color diagram with the region occupied by the stellar locus in the SGP field indicated by the solid line. This is a projection of the multicolor space, but it is a good approximation to the region inaccessible to the multicolor selection technique for redshifts $z \sim 3$. The large symbols show the location of the 55 quasars, redshifts $2.7 < z < 3.5$, from the Lyman-limit survey of Sargent, Steidel, & Boksenberg (1989, hereafter SBB). The colors were derived by multiplying the spectrophotometric data for each quasar by the response functions for each band. The small symbols show the colors of 650 model quasars, redshifts $2.2 < z < 3.5$, for one spectral class ($a = -0.75$, EW Lyα/N v = 84 Å). There is a good match between the domain in this diagram occupied by the SSB quasars, and the domain covered by the model quasars. The few SBB quasars with $m_{b_j} - m_v$ colors bluer than the models have stronger lines, and their colors are well reproduced by the models for the appropriate spectral class.

3.2. *Instrinsic Variability*

Intrinsic photometric variability introduces an effect on quasar colors that we did not account for in our original simulations. A large fraction of the quasar population exhibits brightness variations of $\gtrsim 0.2$ mag on timescales of years (e.g., Bònoli et al. 1979), and as the dates of our plates are separated by differences of up to seven years quasars may appear displaced from their true locations in the multicolor space. When the true position of an object lies well away from the densely populated stellar locus the effect on the detection probability is minimal: The quasar colors are scattered from one low-density region to another, and in both cases the quasar is readily detected. A more significant effect occurs when a quasar is located adjacent to, or coincident with, the volume occupied by the stellar locus. Quasars may be scattered into or out of the stellar locus, in the former case escaping detection while in the latter becoming detectable. The volume of multicolor space occupied by the stellar locus is small, and consequently the number of quasars scattered into the locus is also small. Most important, quasars whose true positions lie within the stellar

© American Astronomical Society • Provided by the NASA Astrophysics Data System

1994ApJ...421..412W

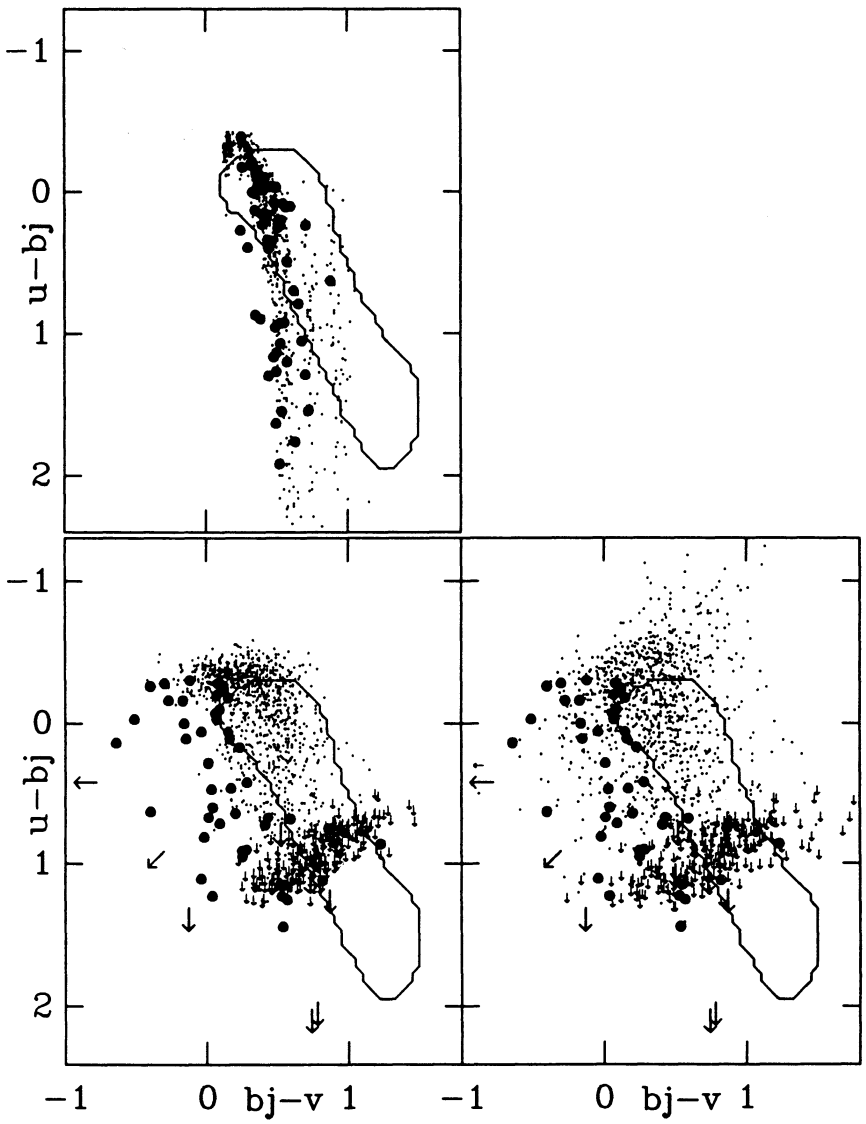

FIG. 1.—Two-color ub_jv diagrams illustrating successively the effects on the detectability of quasars of (*a*) *Top*: line and continuum absorption, (*b*) *Bottom, left side*: photometric errors and plate magnitude limits, (*c*) *Bottom, right side*: quasar variability. The plots compare simulated quasar colors against observed colors. In each plot the solid outline is the domain occupied by normal stars. The simulated colors are for quasars of a particular line strength (EW Lyα/N v = 84 Å) and continuum spectral index ($\alpha = -0.75$), (*a*) Small symbols: 650 model quasars $2.2 < z < 3.5$, line and continuum absorption only, $m_{b_j} - m_v$ increases with redshift. *Large symbols*: colors computed from the spectra of 55 quasars $2.7 < z < 3.5$ observed by SSB. (*b*) *Small symbols*: the same model quasars, including photometric errors, with objects missing off the *u* plates plotted at the color limit, as appropriate for $m_{or} = 19.5$ (the plate limit moves up or down depending on the apparent magnitude). *Large symbols*: the 55 quasars $2.2 < z < 3.5$ in the SGP field, in the complete sample. (*c*) Identical to the previous plot, except here the effects of variability have been included in modeling quasar colors. We did not observe objects $m_u - m_{b_j} \lesssim -0.3$ (see Paper I). The influence of variability on the colors of quasars in our other survey field, F401, is considerably smaller, as the plates for the field were taken over a shorter time span. This diagram is from Warren, Hewett, & Osmer (1991c).

locus, and whose detection probabilities are essentially zero, may be scattered into regions where they are detectable. Failure to take into account the effects of quasar variability results in quasars with supposedly almost zero detection probability being found! Without this correction the actual number of such quasars would be greatly overestimated. The effect is a systematic function of redshift because the location of quasars within the multicolor space is a function of redshift. Quasars with $z \sim 2.7$, which have colors similar to main-sequence turnoff stars, are the most affected (as well as quasars with $z \sim 2.2$, near the ultraviolet excess cut). Incorporating the effects of photometric variability correctly allows for the quasars being scattered out of the stellar locus, raising their detection probabilities.

Appendix B describes the model used to take into account the effects of variability on the observed colors of the quasars. Comparisons of the model predictions with the variability properties of a number of quasar samples are also given. The importance of taking into account the effects of variability is illustrated in Figures 1*b* and 1*c*. Large symbols indicate the colors of quasars detected in one of our survey fields, with arrows showing color limits for quasars not detected in one or more than three passbands. In Figure 1*b* the small symbols show the positions of the same 650 model quasars, redshifts

© American Astronomical Society • Provided by the NASA Astrophysics Data System

1994ApJ...421..412W

$2.2 < z < 3.5$, from Figure 1*a*. However, here the photometric errors have been accounted for, as appropriate for quasars $m_{or} = 19.5$, as well as the plate magnitude limits. In Figure 1*b* the effect of variability was not included. Figure 1*c* is an identical plot except that the colors of the model quasars include the effects of variability. The agreement between the location of the model quasars and the objects detected in the survey is much improved. In particular, significant numbers of model quasars appear to the left of the stellar locus, where the number of detections is large, yet previously few model quasars were evident in this region.

It is clear from this figure that quasar variability had a significant influence on the detectability of quasars in our survey. Therefore the estimate of the luminosity function presented here depends on the accuracy of the model used to generate quasar light curves. In the Appendix we quantify this uncertainty. We show there that, rather than the accuracy of the variability model, it is the limited size of our high-redshift sample which determines the accuracy of the luminosity function results.

It is worth noting that variability will affect the probability of selecting quasars in any color-based survey where the photographic or CCD source material is not all acquired within a period of a few months. The practical consequence of the variability is to blur well-defined color-selection boundaries. The impact of the variability on the detection probabilities depends on where the color-selection boundaries fall relative to the distribution of colors of the quasars sought, and on the epoch difference between the source material.

4. ABSOLUTE MAGNITUDES

Quasar luminosity functions are usually presented in terms of the number of quasars per unit comoving volume per unit absolute blue continuum magnitude, M_B. However, as has been stressed by Schmidt, Schneider, & Gunn (1988), the luminosity of, say, the Lyα/N v emission line may equally well be used to chart quasar evolution, and for surveys limited on line flux (such as theirs) is a more natural measure. Since the line luminosity function and the continuum luminosity function measured different properties, taken separately they provide an incomplete description of the quasar population.

A simple parameterization of the rest-frame ultraviolet SED of a quasar is the continuum luminosity at some specified wavelength, the luminosity of the most important ultraviolet line Lyα/N v, and the continuum spectral index. A more complete description of the quasar population, then, is the distribution in the four-dimensional (4-D) space defined by the parameters: continuum luminosity, line luminosity, continuum spectral index, and redshift. The line luminosity function and continuum luminosity function are simply projections of these data. For samples with well-defined selection criteria, limited either on line flux or broad-band magnitude, it is possible to derive this 4-D distribution, and this is the goal of this paper. Our sample is small, and we will adopt the simplifying assumption that the EW and spectral-index distributions are independent of absolute magnitude and redshift. This supposes, then, that the intrinsic spectral properties of quasars do not evolve with redshift, an assumption considered further in § 7.2.

It is important to be clear what is meant by the EW and spectral-index distributions, as referred to in this paper. These distributions are those that would be measured for a sample comprising all quasars in a given volume, within a specified range of continuum absolute magnitude. Thus this EW distribution is not the same as one found for a quasar sample selected according to a range in line luminosity. Similarly if the absolute magnitudes were referred to a different rest-frame wavelength, the spectral-index distribution would necessarily be different, the difference depending on the shape of the luminosity function.

With the above in mind we present our results in terms of two magnitudes $M_{C(1216)}$ and $M_{L(1216)}$, which are logarithmic measures of the absolute continuum flux under the Lyα/N v

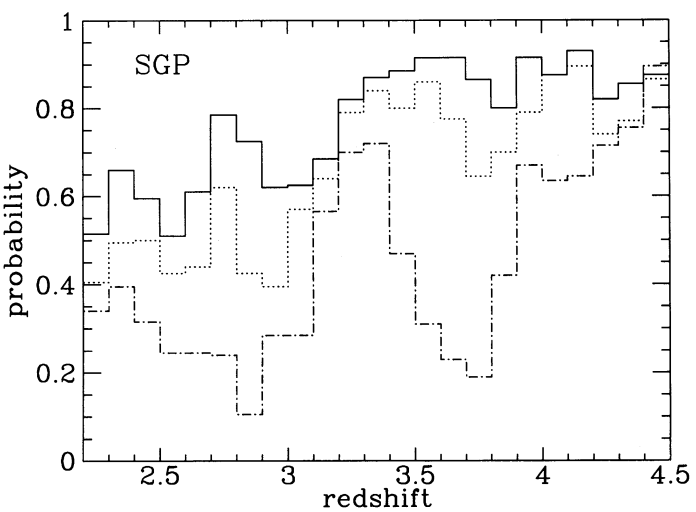

FIG. 2*a*

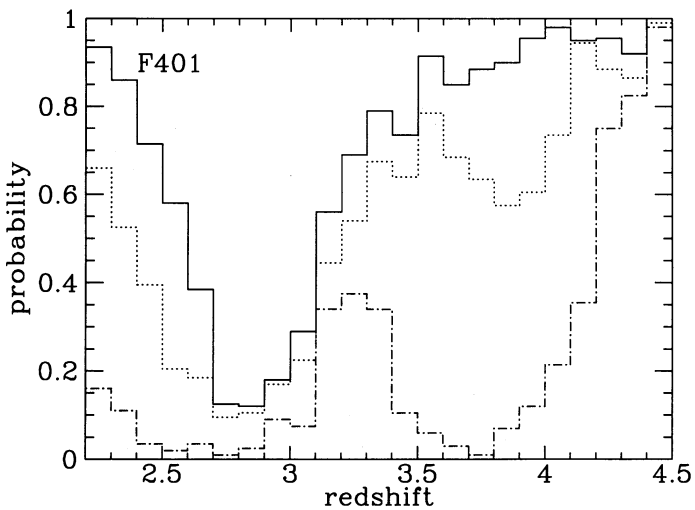

FIG. 2*b*

FIG. 2.—Examples of the revised selection functions illustrating how the detectability of quasars varies as a function of redshift and apparent magnitude, for each of the two survey fields. (*a*) *Left*: SGP field; (*b*) *right*: F401. These plots are for one particular quasar type only, of spectral index $\alpha = -0.75$, and EW Lyα/N v = 84 Å. In each plot the upper, middle, and lower lines are cross sections through the selection functions at apparent magnitudes $m_{or} = 17.0$, 18.0, 19.0 respectively. The general differences between the results for the two fields may be understood as a consequence of the larger number of stars in F401, and of the greater effect of quasar variability for the SGP field, because of the larger time span over which the plates were taken. Thus at faint magnitudes the detection probabilities are considerably lower for F401, while at bright magnitudes for redshifts $z < 2.5$ they are higher because in the SGP more quasars are scattered to colors above the UVX cut.

© American Astronomical Society • Provided by the NASA Astrophysics Data System

1994ApJ...421..412W

emission line, and of the Lyα/N v line luminosity. Here we discuss the advantages of referring absolute magnitudes to a wavelength in the rest-frame ultraviolet, and then define the absolute magnitudes employed.

If the contribution of emission lines to the broadband flux can be neglected, the formula relating M_B and apparent blue magnitude m_B is (Schmidt & Green 1983)

$$M_B = m_B - 5 \log [A(z)c/H_0] + 2.5(1 + \alpha) \log (1 + z) - 25 , \quad (1)$$

where $A(z)c/H_0$ is the bolometric luminosity distance, and the extrapolation from the wavelength observed in the B band, $\lambda_{\text{rest frame}} \sim 4400/(1 + z)$, to the rest-frame B band assumes a power-law representation of the quasar continuum $f_\nu \propto \nu^\alpha$.

When quantifying the *evolution* of the population between two redshifts, if the extrapolation is large it is more important to know the width of the distribution of α than the mean values. Any uncertainty $\epsilon(\alpha)$ in the mean spectral index is reflected in an uncertainty in absolute magnitude, which increases with redshift and introduces an artificial luminosity evolution of the population. For a sample of quasars measured at the same observed wavelength the differential effect between two redshifts z_1, z_2 is $\epsilon(M_B) = 2.5\epsilon(\alpha) \log [(1 + z_2)/(1 + z_1)]$. For the redshift range of our sample $2.2 \leq z < 4.5$ the error is quite small, $\epsilon(M_B) = 0.3$ even for $\epsilon(\alpha) = 0.5$. In other words a small error in the mean value of α has only a small effect on the measured evolution.

A distribution of spectral indices is used in computing the luminosity function, thereby avoiding systematic errors associated with adopting a single value (see, e.g., Giallongo & Vagnetti 1992). For two quasars of the same redshift and apparent magnitude m_{or}, but different spectral index, the difference in absolute magnitude is $\Delta M_B = 2.5\Delta\alpha \log [(1 + z)4400/6400]$ (the effective wavelength of the *or* passband is $\lambda \sim 6400$ Å). For the range $-1.5 < \alpha < 0.0$, which covers most measured values, two quasars at $z = 2.2$ have $|\Delta M_B| = 1.3$, that is, the luminosity function is blurred out by this amount. At $z = 4.5$ the difference is $|\Delta M_B| = 2.2$. With a steep luminosity function, say, a power law of index -3.5, such a magnitude difference corresponds to a change in space density of a factor greater than 100. This illustrates why the spread of continuum spectral indices has a greater effect on the evolution derived than does the uncertainty in the mean spectral index.

Given the importance of establishing the nature of the evolution of the quasar luminosity function at high redshifts we prefer to refer absolute magnitudes to the rest-frame ultraviolet, to minimize the extrapolation in computing absolute magnitudes. By referring the continuum flux to $\lambda = 1216$ Å, the line flux and the continuum flux are directly related, independent of the spectral index, thereby simplifying the parameterization of the quasar SED. Using this definition of absolute magnitude, for quasars with continuum slopes differing by $\Delta\alpha = 1.5$ the difference in absolute magnitude for quasars of the same apparent magnitude m_{or} is now much smaller, $|\Delta M| = 0.8, 0.1$ for $z = 2.2, 4.5$.

We define a continuum absolute magnitude on the AB system:

$$M_{C(1216)} = -48.60 - 2.5 \log F_{\nu(\lambda=1216)} , \quad (2)$$

where $F_{\nu(\lambda=1216)}$ is the continuum flux per unit frequency (ergs s^{-1} cm^{-2} Hz^{-1}) measured under the Lyα/N v line and corresponding to a distance of 10 pc. We define also a second absolute magnitude

$$M_{L(1216)} = M_{C(1216)} - 2.5 \log \text{EW}_{\text{rest frame}} , \quad (3)$$

where $\text{EW}_{\text{rest frame}}$ is the rest-frame *unabsorbed* EW of the Lyα/N v line, in angstroms. By unabsorbed EW we mean the measured EW corrected for Lyman-forest absorption. These parameters will be referred to here as the continuum and line absolute magnitudes, and hereafter we will use simply M_L and M_C. The line absolute magnitude is a logarithmic measure of the luminosity L, and the two are related by

$$M_L = 82.36 - 2.5 \log L \quad (4)$$

for L in ergs s^{-1}. We have adopted this definition of a line absolute magnitude because the conversion from the line luminosity function to the continuum luminosity function is then very simply effected through the EW distribution. It remains to relate absolute and apparent magnitudes.

The absolute magnitude M_C is related to the monochromatic apparent magnitude $m_{c(1216)}$ by the same formula relating M_B and m_B (eq. [1]). The analysis in this paper involves apparent magnitudes measured in two UKST passbands, b_j, and *or*. Further surveys for high-redshift quasars may use the UKST *i* passband, and for reference we have also considered this passband. For a power-law spectrum we find the following relations, obtained by integrating power-law spectra underneath the relevant response functions:

$$m_c = m_{b_j} - 1.45\alpha - 0.07 - k' , \quad (5)$$

$$m_c = m_{or} - 1.80\alpha + 0.18 - k' , \quad (6)$$

$$m_c = m_i - 2.04\alpha + 0.37 - k' . \quad (7)$$

The final term k' in the relations above is a correction for the presence of emission or absorption in the particular passband, defined so that net emission in the band gives a negative value of k'. Values of k' are provided in Tables 1–3 for the three passbands, over the relevant redshift ranges, and for the three line-strength classes used in the luminosity function calculation. At the highest redshifts in the *or* passband these line k-corrections account also for absorption in the Lyα forest, and the values quoted are the average values found from 100 synthetic quasar spectra at each redshift, created with the models used to compute the selection functions (Appendix A).

Equation (6) is used for computing m_c for quasars in our own survey, limited on m_{or}, and to compare against the preliminary results of the survey of Irwin et al. (1991). Equation (5) is used for computing m_c for quasars in the survey of Boyle et al. (1990), and the Large Bright QSO Survey or LBQS (Hewett, Foltz, & Chaffee 1993), both limited on m_{b_j}. The absolute calibration assumes that Vega has $m_V = 0.03$ (Johnson et al. 1966). The relative zero points for the UKST bands were established (Paper I) from the known colors of the Vilnius A0 star. We then scaled this star to the same flux as Vega at $\lambda = 5556$ Å (Hayes & Latham 1975), and assuming $m_V = 0.03$ for this

TABLE 1

LINE k-CORRECTIONS: b_j PASSBAND

	UNABS. EW Lyα/N v		
REDSHIFT	42 Å	84 Å	168 Å
2.05	−0.05	−0.10	−0.20
2.15	−0.08	−0.16	−0.31

© American Astronomical Society • Provided by the NASA Astrophysics Data System

1994ApJ...421..412W

TABLE 2

LINE k-CORRECTIONS: or PASSBAND

REDSHIFT	UNABS. EW Lyα/N v 42 Å	84 Å	168 Å
2.25	−0.03	−0.06	−0.11
2.35	−0.03	−0.06	−0.12
2.45	−0.04	−0.08	−0.15
2.55	−0.03	−0.06	−0.12
2.65	−0.01	−0.02	−0.03
2.75	−0.01	−0.03	−0.05
2.85	−0.05	−0.09	−0.18
2.95	−0.07	−0.14	−0.26
3.05	−0.07	−0.14	−0.27
3.15	−0.08	−0.16	−0.29
3.25	−0.10	−0.19	−0.35
3.35	−0.09	−0.18	−0.33
3.45	−0.04	−0.07	−0.14
3.55	−0.02	−0.03	−0.06
3.65	−0.02	−0.04	−0.08
3.75	−0.05	−0.09	−0.17
3.85	−0.10	−0.20	−0.38
3.95	−0.12	−0.27	−0.51
4.05	−0.09	−0.25	−0.53
4.15	−0.01	−0.19	−0.49
4.25	0.06	−0.15	−0.48
4.35	0.12	−0.13	−0.51
4.45	0.26	−0.02	−0.43

scaled star establishes the zero points for the different passbands.

Combining equations (1) and (6) gives

$$M_C = m_{or} - 5 \log [A(z)c/H_0] + 2.5(1 + \alpha) \log (1 + z) - 24.82 - 1.80\alpha - k' , \quad (8)$$

and similar equations for the b_j and i passbands are easily derived.

The line absolute magnitude is calculated from

$$M_L = M_C - 2.5 \log [\mathrm{EW}_{\mathrm{obs}}/(1 + z)] . \quad (9)$$

Alternatively the equation relating M_L to observed line flux, corrected for absorption, f(ergs s^{-1} cm^{-2}) is

$$M_L = -2.5 \log f - 5 \log [A(z)c/H_0] - 42.83 . \quad (10)$$

5. THE LUMINOSITY FUNCTION

In this section two complementary approaches are employed to derive the luminosity function: a direct estimate using the $1/V_a$ estimator, and a maximum-likelihood model fitting procedure. The former approach provides a direct determination but has the disadvantage that binning the data by redshift and absolute magnitude is required to illustrate the results. Also, objects with small values of the detection probability, p, raise the errors of the results. The latter approach treats the errors optically but requires an assumed parameterization of the luminosity function and the form of the evolution. Consistency between the two approaches gives confidence in the robustness of the results.

TABLE 3

LINE k-CORRECTIONS: i PASSBAND

REDSHIFT	UNABS. EW Lyα/N v 42 Å	84 Å	168 Å
4.05	−0.06	−0.12	−0.23
4.15	−0.07	−0.13	−0.25
4.25	−0.07	−0.14	−0.26
4.35	−0.07	−0.13	−0.25
4.45	−0.07	−0.13	−0.24

5.1. *Estimating the Luminosity Function*

Here we present the results of the binned estimate of the luminosity function over the redshift interval $2.0 \le z < 4.5$, for two values of the deceleration parameter $q_0 = 0.1$, 0.5, and an assumed value of the Hubble constant $H_0 = 75$ km s^{-1} Mpc^{-1}.

Details of the high-redshift quasars employed in the calculation are tabulated in Appendix C. The high-redshift sample comprises the 86 quasars $2.2 \le z < 4.5$ from our own survey, three bright quasars $3.4 \le z < 4.1$ from Mitchell, Miller, & Boyle (1990), and 11 bright quasars $2.2 \le z < 3.3$ from Osmer & Smith (1980). In Figure 3 we plot redshift versus continuum absolute magnitude M_C for these 100 quasars. The thick lines indicate the magnitude and redshift limits for the three surveys. The dotted lines are contours of sample completeness, and the explanation of how they were computed is given later (§ 5.3). For the purposes of this plot and for the binned calculation, values of M_C have been computed assuming $\alpha = -0.75$ and using the line k-corrections for the middle EW bin in Table 2.

The choice of the redshift ranges for the binned estimate was based on an examination of Figure 3, and of the selection functions. The individual selection functions (e.g., Fig. 2) display the same general behavior shown by the contours in this plot, viz., lower detection probabilities in the redshift ranges $2.2 \le z < 3.0$ and $3.5 \le z < 4.0$, and higher probabilities elsewhere. The volume per unit redshift dV/dz changes quite gradually over the redshift interval $2.2 \le z < 4.5$. The main features of the evolution of the luminosity function apparent from Figure 3 are (a) a weak trend toward brighter M_C, at similar space densities, over the interval $2.2 \le z < 3.5$, and (b) a decrease in space density beyond $z = 3.5$. Accordingly we have divided the redshift range of the survey into the three bins $2.2 \le z < 3.0$, $3.0 \le z < 3.5$, $3.5 \le z < 4.5$. The broader redshift intervals of the outer two bins compensate for the lower detection probabilities relative to the central bin.

The subsample from Osmer & Smith (1980) is assumed complete, that is, the detection probability for each of these 11 quasars is $p = 1.0$. We have classified the remaining quasars on the basis of their spectral properties into one of the nine spectral classes, and for each quasar we have extracted the detection probability p from the appropriate selection function. These probabilities are provided in Table 12 (Appendix C).

Finally, to provide an estimate of the luminosity function at lower redshift, $z = 2.1$, against which to compare the high-redshift results we have taken all the quasars of redshifts $2.0 \le z < 2.2$ from the LBQS survey (Hewett et al. 1993) (63 quasars) and the Boyle et al. (1990) survey (47 quasars), and the magnitude limits and effective areas quoted in these references. A bright magnitude limit $m_{b_j} = 16.5$ has been used for the LBQS. These two samples are assumed complete. The apparent magnitudes (m_b) of Boyle et al. (1990) are unconventional but can be transformed to m_{b_j} by a zero-point correction. Boyle et al. calibrated their b_j plates with B standards, of mean color $m_B - m_V = 0.9$. In Paper I we derived the color equation $m_{b_j} = m_B + 0.02 - 0.30(m_B - m_V)$. Accordingly we have converted the magnitudes of Boyle et al. to m_{b_j} with the equation $m_{b_j} = m_b - 0.25$.

© American Astronomical Society • Provided by the NASA Astrophysics Data System

1994ApJ...421..412W

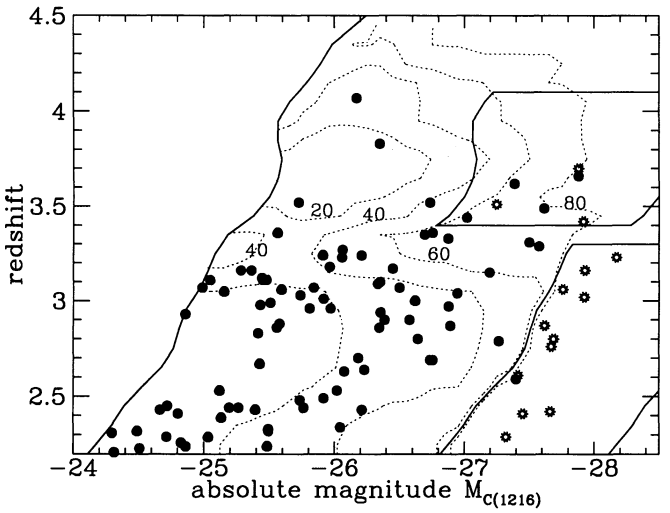

FIG. 3a

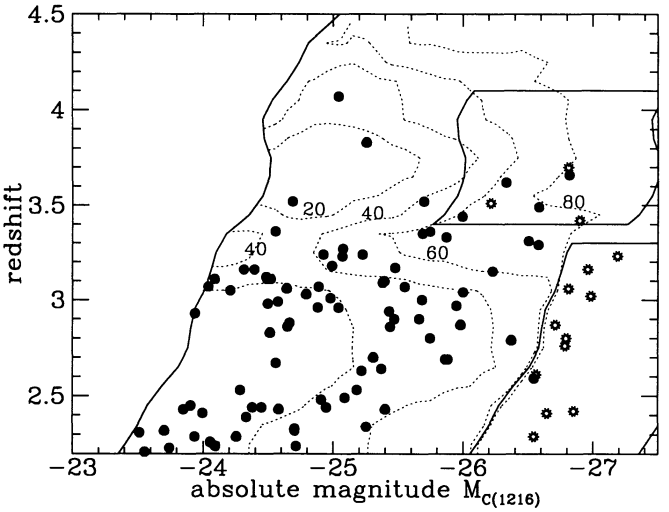

FIG. 3b

FIG. 3.—Redshift vs. continuum absolute magnitude for the 100 high-redshift quasars used in the calculation of the luminosity function. *Top left*: $q_0 = 0.1$; *bottom right*: $q_0 = 0.5$. The sample comprises the 86 quasars from our multicolor survey ($2.2 \leq z < 4.5$, *filled cricles*), three quasars from the survey of Mitchell et al. (1990) ($3.4 \leq z < 4.1$, *open stars*), and 11 quasars from the survey of Osmer & Smith (1980) ($2.2 \leq z < 3.3$, *open stars*). The leftmost solid line is the apparent magnitude limit $m_{or} = 20.0$ of the deeper of the two multicolor-survey fields, the SGP. Other solid lines show the limits of the other two surveys. Further details of the three surveys are provided in Appendix C. The survey completeness, weighted as appropriate for the nine spectral types and the different survey areas, is shown as contour plots at intervals of 20%. Notice that in places the completeness rises near the survey limit. This is because the survey reached deeper in the SGP field (where the completeness is higher) than in F401, and it occurs fainter than the magnitude limit for F401, $m_{or} = 19.68$.

The calculation of space densities proceeds in the usual way using the $1/V_a$ estimator (e.g., Avni & Bahcall 1980), taking into account the redshift- and magnitude-dependent detection probability. Two ways of achieving this are considered. In the first one imagines that the survey is composed of a large number of subsurveys, for each interval $\Delta z = 0.1$, $\Delta m_{or} = 0.1$ (the resolution of the selection functions), and for each spectral type. The area of each subsurvey is the actual area multiplied by the detection probability $p(z, m_{or})$. Thus for each redshift interval, and unit interval in M_C, the space density is computed $\Sigma 1/\int p(z)dV_a$ and the error $[\Sigma 1/\int p(z)dV_a)^2]^{1/2}$. The effective volume computed in this manner then retains the desirable properties of the $1/V_a$ estimator (Felten 1976). This is the procedure we have followed, and the space densities are summarized in Table 4, and plotted in Figure 4.

The second way to estimate the space densities is to correct for incompleteness before computing the available volume. One supposes that for each object found the true number of objects is $1/p$. Thus with this method the space density is computed $\Sigma 1/(pV_a)$ and the error $[\Sigma 1/(pV_a)^2]^{1/2}$. This method produces quite similar results to the first, but the errors are larger. Because the selection functions are so cumbersome they are not provided here, but those who are interested may compute space densities using this alternative method, from the values of p provided in Appendix C.

The appearance of Figure 4 changes somewhat depending on the binning, but the general features remain the same. The behavior of the luminosity function over the redshift interval $2.0 \leq z < 4.5$ is seen to be similar for the two different values of q_0. The nature of the evolution of the luminosity function changes in the third redshift bin $3.0 \leq z < 3.5$. From $z = 2.0$ to $z \sim 3.25$, at bright absolute magnitudes the space density increases uniformly toward higher redshifts, while at fainter M_C the space density changes little between these redshifts. There is a marked decline in the space density of quasars from $z \sim 3.25$ to $z = 4.5$. The smooth transition between the low-redshift data $z < 2.2$ and the high-redshift data $z \geq 2.2$ is evidence that the selection functions are realistic.

5.2. *Maximum-Likelihood Procedures*

We use the maximum-likelihood technique to determine the range of parametric luminosity-function models that are con-

TABLE 4

SPACE DENSITIES

			REDSHIFT RANGE			
q_0	H_0	M_C	$2.0 \leq z < 2.2$	$2.2 \leq z < 3.0$	$3.0 \leq z < 3.5$	$3.5 \leq z < 4.5$
0.1	75.....	−24 to −25	$9.66 \times 10^{-7} \pm 2.42 \times 10^{-7}$	$2.02 \times 10^{-6} \pm 9.28 \times 10^{-7}$	...	...
		−25 to −26	$7.23 \times 10^{-7} \pm 1.84 \times 10^{-7}$	$4.46 \times 10^{-7} \pm 1.07 \times 10^{-7}$	$3.39 \times 10^{-7} \pm 1.04 \times 10^{-7}$	$2.65 \times 10^{-8} \pm 2.65 \times 10^{-8}$
		−26 to −27	$5.44 \times 10^{-8} \pm 8.72 \times 10^{-9}$	$1.53 \times 10^{-7} \pm 4.48 \times 10^{-8}$	$1.19 \times 10^{-7} \pm 3.57 \times 10^{-8}$	$2.51 \times 10^{-8} \pm 1.56 \times 10^{-8}$
		−27 to −28	$1.40 \times 10^{-9} \pm 1.40 \times 10^{-9}$	$5.08 \times 10^{-9} \pm 1.76 \times 10^{-9}$	$2.66 \times 10^{-8} \pm 1.06 \times 10^{-8}$	$4.00 \times 10^{-9} \pm 2.04 \times 10^{-9}$
0.5	75.....	−23 to −24	$4.22 \times 10^{-6} \pm 9.07 \times 10^{-7}$	$7.27 \times 10^{-6} \pm 3.51 \times 10^{-6}$	...	...
		−24 to −25	$2.33 \times 10^{-6} \pm 5.90 \times 10^{-7}$	$1.63 \times 10^{-6} \pm 3.92 \times 10^{-7}$	$1.54 \times 10^{-6} \pm 4.75 \times 10^{-7}$	$9.42 \times 10^{-8} \pm 9.42 \times 10^{-8}$
		−25 to −26	$2.93 \times 10^{-7} \pm 3.89 \times 10^{-8}$	$6.03 \times 10^{-7} \pm 1.61 \times 10^{-7}$	$4.97 \times 10^{-7} \pm 1.45 \times 10^{-7}$	$1.14 \times 10^{-7} \pm 7.07 \times 10^{-8}$
		−26 to −27	$1.63 \times 10^{-8} \pm 8.14 \times 10^{-9}$	$1.58 \times 10^{-8} \pm 5.48 \times 10^{-9}$	$8.46 \times 10^{-8} \pm 3.62 \times 10^{-8}$	$1.77 \times 10^{-8} \pm 9.01 \times 10^{-9}$

© American Astronomical Society • Provided by the NASA Astrophysics Data System

1994ApJ...421..412W

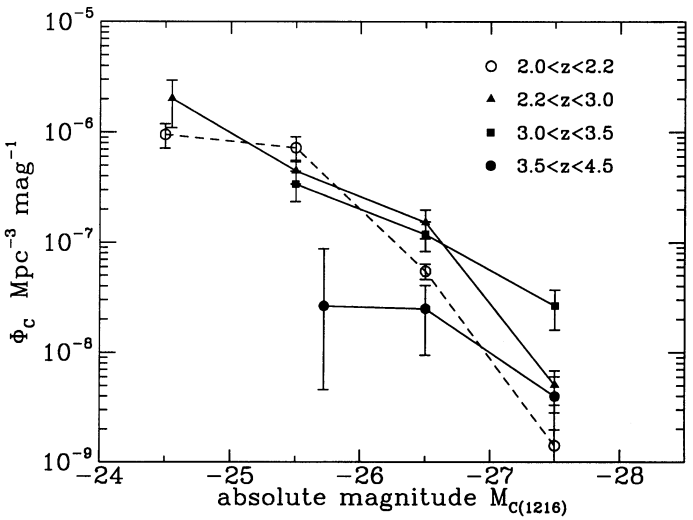

FIG. 4a

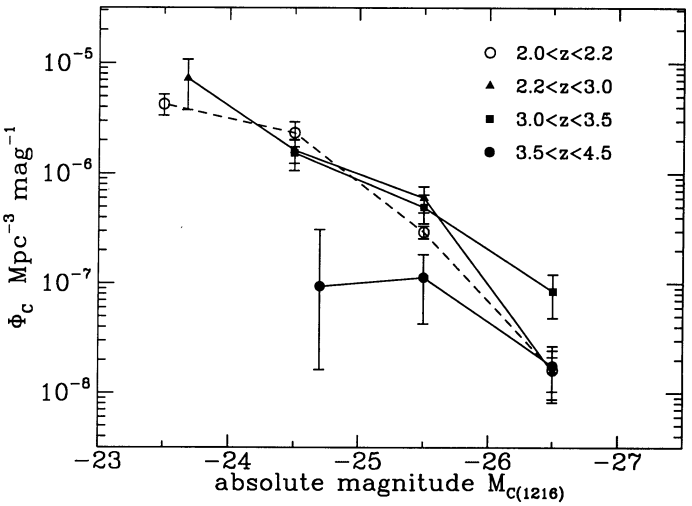

FIG. 4b

FIG. 4.—Binned $1/V_a$ estimate of the continuum luminosity function Φ_c for four redshift intervals over the range $2.0 \leq z < 4.5$. *Left*: $q_0 = 0.1$; *right*: $q_0 = 0.5$. The error bars plotted are the values of σ, Table 4, with the exception of points where only a single object contributes to the space density estimate. For these cases we have plotted the $\pm 34.1\%$ confidence interval (i.e., equivalent of 1 σ for a Gaussian distribution). Bins 1 mag wide were used (Table 4). Each point has been plotted at the central magnitude of the bin (or part bin). (This lies within 0.1 mag of the position where the luminosity function would pass through the point, for power-law luminosity functions less steep than $\alpha = -3.5$.)

sistent with the data. The procedure is described in this section and applied to the data in § 5.3.

The contribution to the binned estimate of the space density, $\propto 1/\int p(z)dV_a$, by quasars with low detection probabilities, $p < 0.10$, is large. Therefore, if a quasar with low detection probability is assigned an incorrect spectral class, the error in the computed space density may be substantial. The signal-to-noise ratio of the spectra (Paper II) of some of the quasars in our sample is inadequate for determining the spectral class with certainty, so the Poisson errors quoted in Table 4 are underestimates of the true errors. The effects of uncertainty in the detection probability for an individual quasar are minimized in the maximum-likelihood calculations because only the total numbers of quasars in each of the nine spectral classes are used, and these numbers must be quite reliable. The determination of the true distribution of spectral classes proceeds as follows. First, a guess is made of the proportion of quasars in each of the nine classes. This distribution is assumed to be independent of absolute magnitude and redshift. For this assumed distribution the maximum-likelihood solution for the luminosity function is determined. From this solution the predicted observed number of quasars in each spectral class is computed and compared against the actual number. This comparison is confined to the multicolor sample as it is the only sample for which the spectral properties have been measured. The initial guess is then revised and a consistent solution reached after a small number of iterations. The proportion of quasars in each class for the multicolor sample is provided in Table 13 (Appendix C), for the two redshift intervals, $2.2 \leq z < 4.5$ and $2.2 \leq z < 3.5$, considered below.

As the selection functions are discrete, $\Delta m_{or} = 0.1$, $\Delta z = 0.1$, the likelihood function to be maximized is a product over bins of this size. Thus for a particular luminosity function we compute the expected number of objects μ_{ij} in each bin over the magnitude and redshift ranges of the high-redshift sample, $20.0 - 0.1(i-1) \leq m_i < 20.0 - 0.1i$, $i = 1, 40$, and $2.2 + 0.1\,(j-1) \leq z_j < 2.2 + 0.1j$, $j = 1, 23$. A similar sum is also made for the low-redshift sample, $2.0 \leq z < 2.2$, when used. The likelihood is the product over all bins of the probability of observing x_{ij} quasars given the expected number μ_{ij}:

$$L = \prod_{i,j} \frac{e^{-\mu_{ij}} \mu_{ij}^{x_{ij}}}{x_{ij}!} . \tag{11}$$

The maximum-likelihood solution is found in each case by minimizing the function:

$$S = -2 \log_e L = -2 \sum_{i,j} x_{ij} \log_e \mu_{ij} + 2 \sum_{i,j} \log_e x_{ij}! + 2 \sum_{i,j} \mu_{ij} . \tag{12}$$

The second term on the right-hand side of this equation may be dropped, as it is independent of the luminosity function. The last term in this expression is simply twice the integral of the luminosity function. In the limit of an infinitesimal bin size all the x_{ij} would be equal to unity where there is a quasar, and zero elsewhere, and equation (12) becomes equivalent to equation (2) of Marshall et al. (1983).

For the parametric luminosity functions a wide range of models was investigated in a similar approach to that of Boyle, Shanks, & Peterson (1988). The goodness of fit was assessed by means of the two-dimensional Kolmogorov-Smirnov (2D K-S) test (Peacock 1983). For the *shape* of the luminosity function we consider both single and double power-law functions, as well as functions of the Schechter form. For the *evolutionary form* both pure-density (PDE) and pure-luminosity evolution (PLE) models were tried. Additionally, for the double power-law and Schechter forms, we considered models in which only the bright end of the luminosity function evolves. We will refer to these models by the acronym PLEB. For the *evolution function* Boyle et al. considered both a power-law function of $1 + z$ and an exponential function of look-back time τ. However, in our case the amount of evolution seen and the interval in look-back time are too small to be able to distinguish between the two functions, and we have restricted ourselves to the exponential form.

Errors on the derived values of the parameters were calcu-

© American Astronomical Society • Provided by the NASA Astrophysics Data System

1994ApJ...421..412W

lated in two ways. The first employs the precepts of Boyle et al. (1988), where, in the n-dimensional parameter space, there is a contour ellipsoid for which $S = S_{\min} + 1.0$. The errors are given by the limits of the projection of this contour ellipsoid on each axis. These limits correspond to the range for normally distributed data containing 68% of values of the parameter in question. Errors quoted in Table 5 are calculated in this fashion.

To verify the validity of this procedure errors using bootstrap techniques (e.g., Barrow, Bhavsar, & Sonoda 1984) were also computed. The bootstrap method mimics the process of repeating the original survey a large number of times. To generate a single artificial survey we selected a random number N from a Poisson distribution of expected value μ, the total number of quasars used in the maximum-likelihood calculation. Then, N times, we selected a quasar at random from the original sample of size μ, to form a new sample. Thus the same quasar could appear more than once in the new sample. The process was repeated 200 times, and for each new sample the maximum-likelihood fit was computed, producing 200 luminosity functions, and 200 estimates for each parameter. For each parameter we found the median value and the upper and lower 34.1% (i.e., 1 σ) quantiles. The errors computed in this way are about 5% larger than those computed in the conventional manner.

The bootstrap error analysis is used additionally in comparing the luminosity function model against the results of other surveys, § 7. The bootstrap analysis allows the error associated with the original fit to be accounted for in such comparisons.

5.3. *The Maximum-Likelihood Model Fits*

We consider firstly the maximum-likelihood solution for models over the entire redshift range $2.2 \leq z < 4.5$, for values of $q_0 = 0.1, 0.5$. All models are ruled out at the 1% level, or better, and the low probabilities are not due to poor fits near the upper or lower redshift limit. This conclusion is consistent with the apparent change in the nature of the evolution at $z \sim 3.25$ evident from the binned estimates of § 5.1, (Fig. 4).

Next we present the best-fit models over the redshift range $2.0 \leq z < 3.5$, which includes 92 of the 100 high-redshift quasars. The inclusion of the low-redshift data $2.0 \leq z < 2.2$ has two motivations. First, because of the larger sample size it improves the constraints on the model fits. Second, it provides a check on whether the selection functions are realistic. The goodness of fit of the model is assessed separately for the low- and high-redshift data. If the selection functions are inaccurate it would be unlikely that a simple model luminosity function provide a satisfactory fit to both data sets.

The maximum-likelihood analysis of the joint sample confirms the indications from the binned analysis, § 5.1. All evolving single power-law models and all nonevolving curved models are excluded at the level of 2% or better. Again the low probabilities are not due to poor fit just near the upper or lower redshift limit. Only evolving curved models remain viable. Because of the shallow faint-end slope, and the restricted redshift range, the PLE and PLEB models are very similar. Both forms provide acceptable fits, and these models are also interesting as they appear to extend the luminosity evolution seen at low redshifts. The PLEB models are slightly preferred over the PLE models in terms of the K-S probabilities. On the other hand the acceptability of the PDE models is marginal, and the models do not join on smoothly to the data at low redshift. Accordingly we restrict attention now to the following two PLEB luminosity functions.

The first is an evolving Schechter function that is the exponential evolutionary form analog of the power-law evolutionary form model of Fall & Pei (1989). In this model the space density remains constant for faint quasars, but evolves for bright quasars. The model is parameterized as follows:

$$\Phi_C(M_C, z)dM_C\,dV = \Phi_C^* 10^{0.4(M_C^* - M_C)(\alpha+1)} \times \exp\left[-10^{0.4[M_C(z) - M_C]}\right]dM_C\,dV \quad (13)$$

where

$$M_C(z) = M_C^* - 1.086k_L\tau\,. \quad (14)$$

The second model is the double power-law PLE exponential model of Boyle et al. (1988), modified such that only the bright power law evolves. This model is parameterized (using the same notation) by

$$\Phi_C(M_C, z)dM_C\,dV = \frac{\Phi_C^*}{\left[10^{0.4[M_C - M_C(z)](\alpha+1)} + 10^{0.4(M_C - M_C)(\beta+1)}\right]}\,dM_C\,dV\,. \quad (15)$$

The best-fit values for the four parameters for the Schechter model, and for the five parameters for the double power-law model are provided in Table 5. The best-fit evolving double power-law luminosity functions are plotted in Figure 5, for the redshifts $z = 2.1$, 2.6, and $z = 3.25$, and may be compared against Figure 4. In Figure 5c we show the 1 σ error on the luminosity function at $z = 3.25$, for $q_0 = 0.5$, determined by the bootstrap method. For each value of q_0 the quality of the best fits for the two models are virtually identical. Although the Schechter models are preferred since they require one less parameter, the double power-law model provides a more direct comparison with the low-redshift luminosity function of Boyle et al. (1988). Accordingly, for the remainder of the paper we refer only to the double power-law models (eq. [15]). However, we have verified that our conclusions regarding the decline in space density at high redshifts are independent of whether the Schechter or the double power-law models are used (or indeed whether the PLE or PLEB forms are adopted).

The large errors for k_L (Table 5) are a consequence of the small range in look-back time, while the large errors in M_C^*, are a consequence of the coupling with k_L in equation (14), and the difficulty in locating the break in the luminosity function when only sampling intermediate magnitudes. This difficulty of fixing the position of the break means also that the errors on the parameters α and β are strongly correlated. Although the values of α and β are significantly more negative than those found by Boyle et al. (1990) for lower redshifts, this may be a consequence of the restricted magnitude range of our data. In other words it is possible that the slope of the luminosity function becomes shallower at fainter magnitudes.

The models provide an excellent fit to the combined low-redshift sample, $2.0 \leq z < 2.2$, with K-S probabilities $p_{KS} > 70\%$. Nevertheless there is a discrepancy apparent between the results of the LBQS and of the survey of Boyle et al. in this redshift range. Our best-fit model lies slightly above the LBQS data near the magnitude limit of that survey, $m_{b_j} \sim 18.7$, and below the Boyle et al. data at a magnitude $m_{b_j} \sim 19.5$. Our model provides a poor fit to the Boyle et al. sample alone, with $p_{KS} < 3\%$. However, adjusting the relative numbers in the two low-redshift surveys to achieve consistency has no significant

© American Astronomical Society • Provided by the NASA Astrophysics Data System

1994ApJ...421..412W

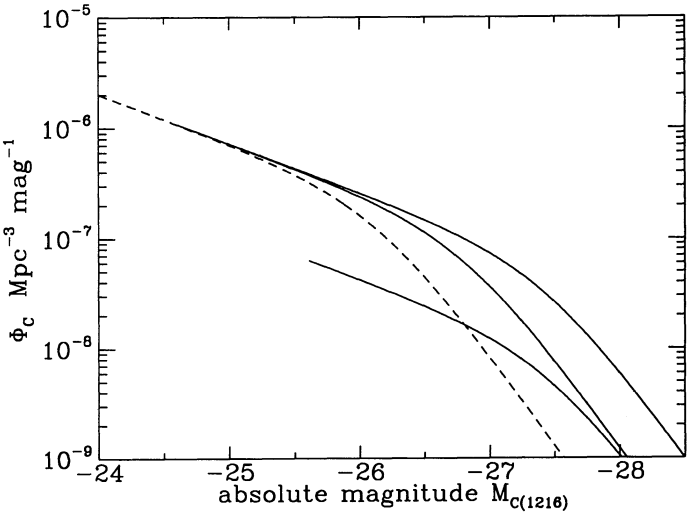

FIG. 5a

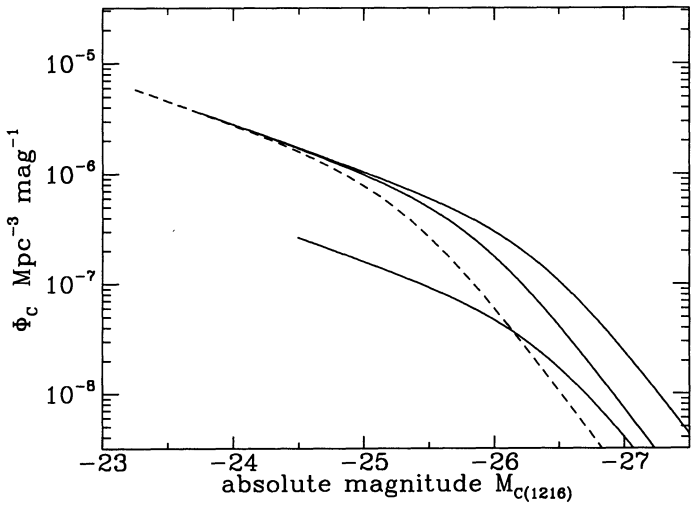

FIG. 5b

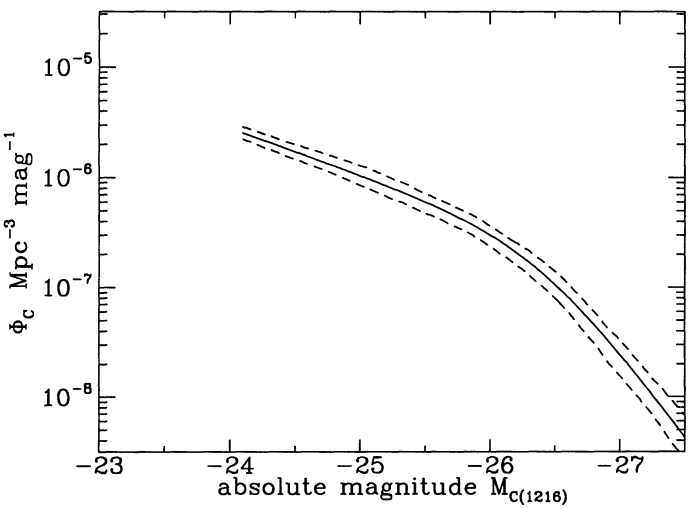

FIG. 5c

FIG. 5.—Best-fit double power-law continuum luminosity function models Φ_C. *Left*: $q_0 = 0.1$; *right*: $q_0 = 0.5$. The four redshifts are the mean redshift of each of the four intervals plotted in Fig. 4, i.e., $z = 2.1$ (*dashed*), $z = 2.6$ (*solid, upper, left*), $z = 3.25$ (*solid, upper, right*), $z = 4.0$ (*solid, lower*). Each line is plotted down to the faint absolute magnitude that corresponds to the apparent magnitude limit $m_{or} = 20.0$. To plot the line at $z = 4.0$ we have divided the luminosity function at $z = 3.3$ by the factors 6.1 (6.5), for $q_0 = 0.1$ (0.5). *Bottom*: the line for $z = 3.25$, $q_0 = 0.5$, together with the 1 σ range, determined in the bootstrap analysis.

effect on our results at higher redshifts $z > 3$, so we will not consider this problem further here.

The 2D K-S probabilities for the high-redshift data, for the double power-law models, over different redshift ranges, are summarized in Table 6. These probabilities fall rapidly as the upper-redshift limit for the comparison is increased from $z = 3.0$ to $z = 3.5$, suggesting that the positive luminosity evolution ceases near a redshift $z \sim 3.3$.

The inferred true proportions of quasars in the nine spectral classes were found to be the same for all models and are listed in Table 7. These are the proportions of quasars that would be found in each class in a complete sample that is limited on M_C. A sample limited on, say, M_B would show a different distribution, with, for example, the spectral-index distribution skewed toward more negative spectral indices. The numbers in Table 7 are also not the proportion of quasars that would be found in a complete sample limited on apparent magnitude, since the apparent magnitude limit corresponds to a different continuum absolute magnitude limit for quasars of different spectral index and EW.

The luminosity function, together with the distribution of spectral types listed in Table 7, specify completely the distribution of quasars in the 4-D space with axes M_C, M_L, α, z. The calculation of the line luminosity function from the continuum luminosity function is detailed in § 7.2.

The dotted lines in Figure 3 are contours of sample completeness, that is, the ratio of the product of the luminosity function and the selection functions (weighted by spectral type), to the total number that actually exists (given by the

TABLE 5

MAXIMUM-LIKELIHOOD SOLUTIONS

EVOLVING SCHECHTER MODEL			DOUBLE POWER-LAW MODEL		
Parameter	$q_0 = 0.1$	$q_0 = 0.5$	Parameter	$q_0 = 0.1$	$q_0 = 0.5$
α	$-1.87^{+0.2}_{-0.1}$	$-1.79^{+0.2}_{-0.2}$	α	$-5.18^{+0.5}_{-0.7}$	$-5.05^{+0.5}_{-0.7}$
M^*_C	$-16.53^{+1.6}_{-1.5}$	$-15.22^{+1.9}_{-1.8}$	β	$-2.11^{+0.1}_{-0.1}$	$-2.06^{+0.2}_{-0.2}$
k_L	$11.34^{+2.0}_{-1.8}$	$11.02^{+2.2}_{-2.0}$	M^*_C	$-14.65^{+1.8}_{-1.9}$	$-13.21^{+2.3}_{-2.3}$
$\log_{10} \Phi^*_C$	$-3.03^{+1.0}_{-0.8}$	$-2.62^{+1.1}_{-0.8}$	k_L	$10.33^{+1.7}_{-1.8}$	$10.13^{+2.0}_{-2.0}$
			$\log_{10} \Phi^*_C$	$-1.55^{+1.2}_{-1.2}$	$-0.99^{+1.5}_{-1.4}$

© American Astronomical Society • Provided by the NASA Astrophysics Data System

1994ApJ...421..412W

TABLE 6

KOLMOGOROV-SMIRNOV TEST PROBABILITIES

	Redshift Range		
q_0	$2.2 \leq z < 3.0$	$2.2 \leq z < 3.3$	$2.2 \leq z < 3.5$
0.1.....	0.414	0.147	0.011
0.5.....	0.426	0.159	0.012

luminosity function). This ratio depends weakly on the shape of the luminosity function (because of the photometric errors), but not on the normalization, and has been computed using the two power-law maximum-likelihood fits of this section, assuming that the shape of the luminosity function for redshifts $z > 3.3$ is the same as at $z = 3.3$.

5.4. *The Decline at High Redshift, $z > 3.5$*

To reiterate, the main conclusions from the previous section are (1) simple models, including pure luminosity or density evolution of a Schechter or double power-law luminosity function, over the entire redshift range $2.2 \leq z < 4.5$ are ruled out. (2) The character of the evolution of the quasar population changes near the midpoint of this redshift interval, that is, $z \sim 3.3$. There are more bright quasars at $z = 3.3$ than at $z = 2.0$. There are fewer quasars at redshifts $z > 3.5$ than at $z = 3.3$. (3) For redshifts $2.0 \leq z < 3.5$, nonevolving models are excluded. (4) For redshifts $2.0 \leq z < 3.5$, PLEB models provide a satisfactory fit. The evolution ceases near $z = 3.3$, and the space density of quasars declines beyond.

The existence of a decline in the space density of quasars at redshifts $z > 3.5$ is the main result of this paper, and here we derive quantitative limits to the size of this decline. We have compared the number of quasars observed at redshifts $3.5 \leq z < 4.5$ with the number expected if the luminosity function ceases to evolve at $z = 3.3$ and remains constant at higher redshifts. The integration, as always, accounts for the distribution by spectral class, the line k-corrections, the photometric errors, and the probability of detection. Compared to the eight quasars found with $z \geq 3.5$, the predicted numbers are 49 and 52 for $q_0 = 0.1, 0.5$.

In the absence of any error in the estimate of the luminosity function at $z = 3.3$ the significance of the decline may be established assuming Poisson errors. For example, for $q_0 = 0.5$ one could say that at the 95% confidence level the decline is greater than 52/14.43, because if the expected number of quasars is 14.43 there is a 5% chance of observing eight quasars or less.

TABLE 7

TRUE DISTRIBUTION OF SPECTRAL TYPES

Spectral Index	Class	Equivalent Width Lyα/N v	$2.2 \leq z < 3.5$
$0.0 < \alpha < -0.5$.....	1	42	0.134
	2	84	0.145
	3	168	0.039
$-0.5 < \alpha < -1.0$.....	4	42	0.231
	5	84	0.319
	6	168	0.040
$-1.0 < \alpha < -1.5$.....	7	42	0.028
	8	84	0.038
	9	168	0.026

Using the bootstrap analysis one can also account for the errors in the fit of the luminosity function. Thus for each value of q_0 we have 200 estimates of the luminosity function at $z = 3.3$, and hence 200 predictions for the number of quasars in the redshift interval $3.5 \leq z < 4.5$. We need to find what factor these numbers should be divided by such that when convolved with the Poisson distribution the proportion of cases where eight quasars or less are observed, corresponds to the desired confidence interval. We find that dividing by a factor 3.1(3.3), for $q_0 = 0.1(0.5)$, in 5% of cases one would expect to observe eight quasars or less.

In conclusion the integrated space density of quasars $M_C < -25.6(< -24.5)$, $q_0 = 0.1(0.5)$, at $z = 4.0$ is lower relative to $z = 3.3$ by an estimated factor of 6.1(6.5). At the 95% confidence level the decline is by a factor $> 3.1(> 3.3)$. These limits are very similar to those found by Osmer (1982).

As a preliminary parameterization of the decline at redshifts $z > 3.3$ we assume a PDE model such that the luminosity function has the same shape as at $z = 3.3$ but is lower by a factor $\exp[(3.3 - z)k_D]$. Values of $k_D = 3.22^{+1.0}_{-0.9}(3.33^{+1.0}_{-1.0})$ for $q_0 = 0.1(0.5)$, respectively, reproduce the number of quasars observed in the interval $3.5 \leq z < 4.5$. In Figure 5, as an indication of the quasar luminosity function at $z = 4.0$, we have shifted the luminosity function at $z = 3.3$ down in density by the factors 6.1(6.5).

6. LOWER LIMITS TO THE SPACE DENSITY AT $z = 3$ AND 4

More high-redshift quasars in the SGP field are known in addition to those in the complete sample, and combined with the complete sample they provide a firm lower limit to the space density at any redshift. Notwithstanding the evidence presented in § 5 and Appendix B that the selection functions are reliable, the corrections made for sample incompleteness are substantial. Therefore we have verified that the number of quasars predicted by our model is consistent with the total number of high-redshift quasars discovered in the fields by all techniques. In this section we compare the results of the luminosity function calculation against the total number of quasars found in the SGP by all techniques and published or known to us, for the intervals $2.8 \leq z < 3.2$ and $3.8 \leq z < 4.2$. We then consider the implications for the reliability of the selection functions, and for the conclusions of the previous section.

The SGP field provides a more stringent check on our model than F401 because (1) the sample of quasars is larger than in F401, (2) several additional high-redshift quasars (Paper II) were found in this field in exploring the multicolor catalogs deeper than the selection criteria defined for the complete sample, and (3) the field has been explored extensively by several other groups. We consider all the known quasars in the SGP field that could have been selected from the multicolor catalog, of effective area 23.5 deg^2 (Paper I, § 3.7). These are the quasars listed in Table 4, Paper I, and Table 2, Paper II, and include a few quasars discovered by others using a variety of techniques (most of these were recovered by the multicolor survey). In addition we have recently found another high-redshift quasar in the SGP, of apparent magnitude $m_{or} = 19.81$, $z = 3.07$. The coordinates of this quasar are R.A. $0^h42^m5^s.76$, decl. $-27°54'44''$ (1950.0 equinox). The total numbers of quasars in the redshift intervals $2.8 \leq z < 3.2$, $3.8 \leq z < 4.2$ are therefore 36 and 3, respectively. (In comparison the numbers of quasars in the complete sample in the SGP field over these redshift intervals are 25 and 1.)

We have computed the expected numbers of quasars over

© American Astronomical Society • Provided by the NASA Astrophysics Data System

1994ApJ...421..412W

these redshift intervals from the best-fit double power-law luminosity functions, again integrating over the distribution of spectral types, and allowing for the photometric errors. For redshifts $z > 3.3$ we assume an exponential decline using the parameterization of § 5.4. In Table 8 we compare the predicted numbers in the survey area against the numbers found. These results are essentially independent of q_0 (since the prediction uses a luminosity function fit to data in the same redshift interval).

There are two ways of interpreting the results summarized in Table 8. If the luminosity function parameterization of § 5 is correct, then, in the redshift interval $2.8 \leq z < 3.2$, there remain only a few bright $m_{or} \leq 19.0$ quasars in the SGP to be found, and at fainter magnitudes $20.0 \geq m_{or} > 19.0$ about 60% of the quasars in this redshift interval have been discovered. The low completeness is plausible when it is recalled that the brightest known quasar in the SGP in this redshift range ($m_{or} = 17.80$, $z = 3.04$, Paper I, Table 4) is not in our complete sample! Qualitatively, the implied level of completeness accords with expectation, which argues that the selection functions are reasonable. A scond interpretation produces a firm lower limit to the luminosity function at redshift $z = 3$ by taking the model prediction of § 5, multiplied by the ratio of the number of objects found to the number of objects predicted (Table 8). For $z = 3$ at bright absolute magnitudes the model luminosity function lies about an order of magnitude higher than at $z = 2.1$. Therefore there is compelling evidence for continued evolution of the luminosity function, to brighter luminosities, beyond $z = 2$.

In the higher redshift interval, $3.8 \leq z < 4.2$, three quasars have been found, and the model predicts ~ 3. Therefore the lower limit to the space density of quasars of redshift $z \sim 4$ is about equal to the number predicted in § 5.

7. COMPARISON WITH OTHER SURVEYS

7.1. *Predictions for the Survey of Irwin et al.*, $4.0 \leq z < 4.5$

Irwin et al. are undertaking a survey for bright quasars of redshifts $z \geq 4$ using UKST plates. This survey is ongoing but preliminary results from the first 2500 deg^2 have been obtained (Irwin et al. 1991, and private communication). In the first ~ 1000 deg^2 of the survey single b_j, *or*, and *i* plates were used, and the redshift range $4.0 \leq z < 4.7$ was targeted. In the second ~ 1500 deg^2, using just b_j and *or* plates, quasars with redshifts $z > 4.2$ were sought by restricting follow-up spectroscopy to the reddest candidates, objects with $m_{b_j} - m_{or} \gtrsim 3$. Some 25 quasars with $z > 4$ have been confirmed. The precise effective area, magnitude limits, and number of quasars found have not been published, but we will assume an effective area of 1000 deg^2 (i.e., a completeness of 40%, bearing in mind that spectroscopy of candidates is not yet complete), an apparent magnitude range $16.0 \leq m_{or} < 19.0$, and the redshift range $4.0 \leq z < 4.5$.

The predictions are summarized in Table 9, where we have

TABLE 8

PREDICTED TRUE NUMBERS VERSUS NUMBER FOUND SO FAR

REDSHIFT RANGE	FAINT $m_{or} > 19.0$		BRIGHT $m_{or} \leq 19.0$	
	Predicted	Found	Predicted	Found
$2.8 \leq z < 3.2$.....	41	25	16	11
$3.8 \leq z < 4.2$.....	2.4	3	0.7	0

TABLE 9

NUMBERS PREDICTED FOR THE SURVEY OF IRWIN ET AL., $4.0 \leq z < 4.5$

	LUMINOSITY FUNCTION MODEL		
q_0	$z = 3.3$ Fixed	$z = 3.3$ Exp. Decline	$z = 2.1$ Fixed
0.1.....	214^{+46}_{-44}	13^{+18}_{-8}	20^{+8}_{-6}
0.5.....	242^{+51}_{-50}	13^{+19}_{-8}	49^{+23}_{-12}

computed the expected numbers for three different model luminosity functions. The first column corresponds to the calculation presented in § 5.4 where we have supposed that the luminosity function ceases to evolve at $z = 3.3$ and remains constant thereafter. The errors quoted are the bootstrap errors (i.e., the errors associated with the uncertainty of the luminosity function at $z = 3.3$) convolved with the Poisson distribution. The predicted number of quasars, over 200, greatly exceeds, and is incompatible with, the number found. Our preliminary conclusion is that the space density of bright quasars, $M_C < -27(-26)$, $q_0 = 0.1(0.5)$ is lower at $z \sim 4.3$ relative to $z = 3.3$ by a factor ~ 9.

In the second column of Table 9 we provide the predicted number assuming the exponential model for the decline beyond $z = 3.3$ put forward in § 5.4. Here the uncertainty in the parameter k_D is also accounted for in the error analysis. The predictions of the model are consistent with the number of quasars found, but the 1 σ range is large. Another way of comparing the results is to compute the values of k_D that yield 25 quasars for the survey of Irwin et al. We find $k_D = 2.43$ (2.56), for $q_0 = 0.1(0.5)$. These values lie within the 1 σ range of k_D found from our own survey. In conclusion, the results of the two surveys both indicate a strong decline in the space density of quasars beyond $z = 3.3$ and are consistent with a decline that is independent of absolute magnitude.

Irwin et al. (1991) have proposed that the space density of bright quasars at $z \sim 4.3$ is similar to that at $z \sim 2$. In the third column of Table 9 we provide the expected number of quasars if the luminosity function in the redshift range $4.0 \leq z < 4.5$ were the same as at $z = 2.1$. For $q_0 = 0.1$ the predicted number is similar to the number found, but a decline between $z = 2.1$ and $z = 4.3$ is indicated for $q_0 = 0.5$.

The foregoing comparison is provisional as the conclusions depend quite sensitively on the exact magnitude limit of the survey. For a change in limiting magnitude of only 0.2 mag the predicted numbers change by some 40% for the first two models, and by even more for the last.

7.2. *Predictions for the Survey of Schmidt et al.: The Line Luminosity Function at $z = 3$ and 4*

Schmidt et al. (e.g., 1987, 1988, 1991) have completed a slitless spectroscopic survey for high-redshift quasars, of similar area and depth to our multicolor survey. As discussed in § 4 it is possible to derive both the line and continuum luminosity functions for such a survey, without reference to other samples. The line luminosity function is the easier to derive, as their sample is limited on line flux. Here we provide a prediction for comparison with their results, when available, based on the models of § 5.4, in the form of the line luminosity function at $z = 3$ and 4. To date they have concentrated on estimates of the space density at high redshifts.

As mentioned in § 5.3 the continuum luminosity function Φ_C

© American Astronomical Society • Provided by the NASA Astrophysics Data System

1994ApJ...421..412W

(Table 5) together with the distribution of spectral types (Table 7) specify completely the distribution of quasars in the 4-D parameter space with axes M_C, M_L, α, z. The calculation of the Lyα/N v line luminosity function Φ_L from Φ_C involves a straightforward summation over the Lyα/N v EW distribution Ψ(EW), because of the simple relation between M_L and M_C (eq. [3]). For this calculation, at faint M_C, where the slope of the luminosity function is shallow, the shape of Ψ(EW) is not critical, and $\Phi_L(M_L) \approx \Phi_C(M_L + 2.5 \log \mathrm{EW_{med}})$, where $\mathrm{EW_{med}}$ is the median EW. However at bright magnitudes, because of the slope, objects of the same M_L of different EW correspond to very different values of Φ_C, and it is necessary to know the distribution Ψ(EW) accurately. The division of the EW distribution into only three bins (Table 7) is too coarse, and here we first obtain Ψ(EW) at higher resolution.

The observed distribution of spectral types (Table 13) for the redshift range $2.2 \leq z < 3.5$ was obtained from the properties of the 70 quasars in this redshift range which have measurements of both the spectral index and the Lyα/N v EW, corrected for absorption. The proportion of objects in the three EW bins is shown in Figure 6*a* (*dotted*), together with the inferred true distribution (*solid*). The ratio of the two values is a correction factor to the observed distribution, and by assuming that this factor does not vary across a bin this correction may be applied to the observed distribution on a finer binning. This amounts to the assumption that the detection probability of two quasars of the same redshift, apparent magnitude, and spectral index is approximately the same for the range of EWs across any bin.

The resulting inferred true EW distribution for six bins, of half the original size, is shown in Figure 6*b*. The relative numbers of objects in each bin, from left to right are 0.131, 0.262, 0.298, 0.203, 0.077, 0.028, and are assumed to be distributed uniformly logarithmically across each bin. In Figure 7 we plot the line luminosity functions for $z = 3$ and $z = 4$, calculated for this EW distribution. To compute the line luminosity function at $z = 4$ we assumed the exponential decline for the continuum luminosity function, put forward in § 5.4. For comparison, the preliminary results of Schmidt et al. (1991) give a decline of a factor of 3.2 per unit redshift.

The EW distribution of Figure 6*b* resembles the symmetric log-triangular function proposed by Schmidt, Schneider, & Gunn (1986). The function is characterized by the median value $\mathrm{EW_{med}}$, and the ratio of the maximum and minimum values $\mathrm{EW_{max}/EW_{min}}$. Adopting their value of 10 for this ratio, and a value $\mathrm{EW_{med}} = 68$ Å and calculating the line luminosity function for this distribution, we find that the results agree with those for the binned EW distribution to within a few percent, over the magnitude ranges of interest. Therefore the log-triangular distribution provides a convenient analytic function for such calculations. The value of $\mathrm{EW_{med}}$ is almost identical to that of the binned distribution.

We turn now to the question of spectral evolution, raised in § 4. In assessing the decline in space density at high redshift we have supposed that the true distribution of spectral properties for redshift $z > 3.5$ is the same as for redshifts $2.2 \leq z < 3.5$. Our sample of quasars $z > 3.5$ is too small to test for evolution. However, it will be possible to make this test once the sample of Irwin et al. (1991) is published, as we can compute the expected distribution of spectral properties for their sample. In the meantime we consider whether the main conclusions of this paper would be affected if spectral evolution is present.

For the calculation of the continuum luminosity function spectral evolution enters in two ways, both indirect: through the detection probability, and through the line k-corrections. Both these effects are relatively minor, since the detection probabilities do not change dramatically between the different spectral classes, and because the line k-corrections are not large. Given that the spectral properties of the quasars of $z > 3.5$ in our sample are not unusual, we can conclude that any spectral evolution that does occur beyond $z > 3.5$ will have only a minor effect on our conclusions regarding the decline of the continuum luminosity function.

With regard to the estimate of the line luminosity function at

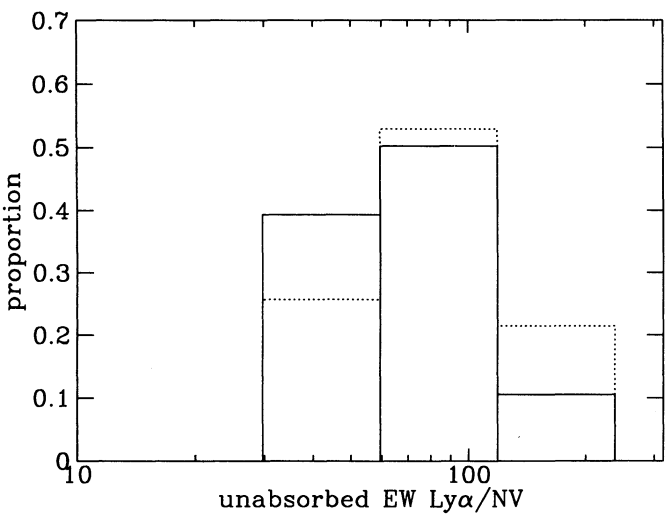

FIG. 6*a*

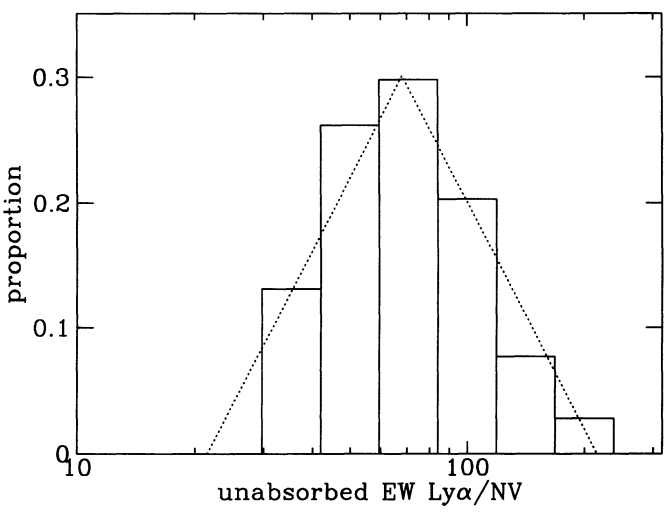

FIG. 6*b*

FIG. 6.—(*a*) *Left*: *Solid line*: the inferred true EW distribution $2.2 \leq z < 3.5$ for a sample limited on absolute magnitude M_C. *Dotted line*: the observed EW distribution for the 70 quasars $2.2 \leq z < 3.5$ in the complete sample, with measured EWs and spectral indices. The bins are spaced equally logarithmically, centered on EW = 42, 84, 168 Å. (*b*) *Right*: Solid line, the derived true EW distribution for EW bins half as large as in (*a*). Dotted line, a symmetric log-triangular distribution, of range $\mathrm{EW_{max}/EW_{min}} = 10$, and median value $\mathrm{EW_{med}} = 68$ Å, which may be used as an alternative to the binned distribution, for computing the line luminosity function.

© American Astronomical Society • Provided by the NASA Astrophysics Data System

1994ApJ...421..412W

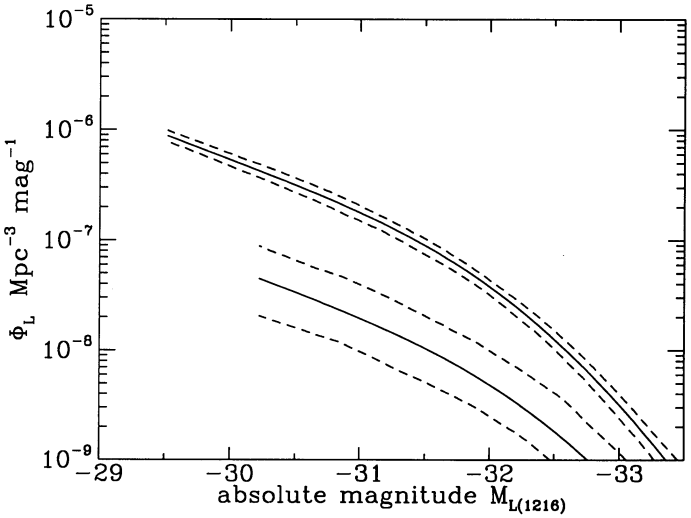

FIG. 7a

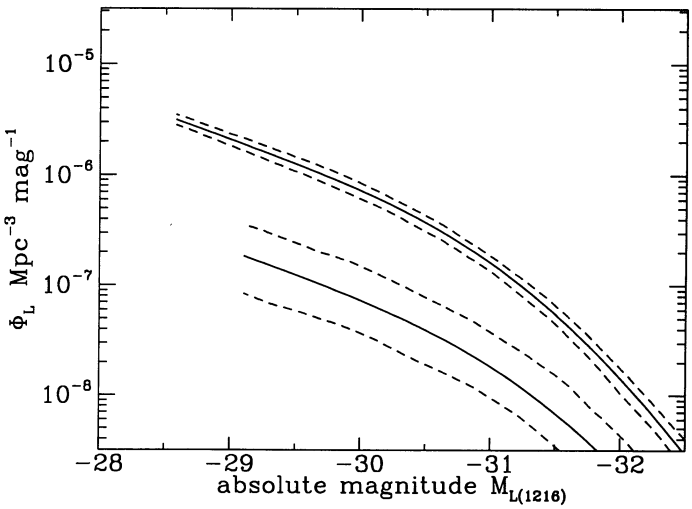

FIG. 7b

FIG. 7.—Line luminosity function Φ_L at $z = 3$ (*upper solid line*), and $z = 4$ (*lower solid line*), and the 1 σ range. *Left*: $q_0 = 0.1$; *right*: $q_0 = 0.5$.

$z = 4$ (Fig. 7), here the effect of evolution of the EW distribution is direct and could be important. Thus, if Ψ(EW) shifts toward weaker EWs our prediction is an overestimate of Φ_L, and vice versa. A discrepancy between the prediction of Φ_L at $z = 4$ and the results of the survey of Schmidt et al. would be an indication of such spectral evolution. Evolution of the spectral-index distribution, however, does not affect the calculation of Φ_L from Φ_C.

8. CONCLUSIONS

We have investigated the evolution of the quasar luminosity function over the redshift range $2.0 \leq z < 4.5$ using our complete sample of 86 quasars, obtained from a multicolor data set using precisely specified selection criteria, combined with other published samples. The luminosity function is presented in terms of the monochromatic continuum absolute magnitude beneath the Lyα/N v emission line, M_C. The calculation deconvolves the selection biases in the sample, and at the same time the true distribution of spectral properties is derived, thereby providing a complete description of the quasar population in the M_C, M_L, α, z parameter space. The calculation accounts for the variation in detectability of quasars as a function of apparent magnitude, redshift, line strength, and continuum slope. The calculation accounts also for the effect of the photometric errors, and the quasar apparent magnitudes are corrected for the effect of emission and absorption lines. Finally, new estimates of the effect of absorbing clouds along the line of sight and of the variability of quasars on their detectability were made in this paper and applied to the derivation of the luminosity function.

The main conclusions are as follows:

1. No single simple parameterization of the luminosity function fits the behavior of the data over the entire redshift interval $2.2 \leq z < 4.5$.

2. There is strong evidence for positive evolution of the quasar luminosity function from $z = 2.0$ to about $z = 3.3$. There are more bright quasars at $z = 3.3$ than at $z = 2.0$, but similar numbers of faint quasars. Curved luminosity-evolution models, in which only the bright end evolves, give a good fit to the data.

3. The space density of quasars declines for redshifts $z > 3.3$. The space density of quasars with $M_C < -25.6(< -24.5)$, $q_0 = 0.1(0.5)$, at $z = 4.0$ is estimated to be a factor of 6.1(6.5) less than at $z = 3.3$. At the 95% confidence level, the decline is greater than a factor of 3.1(3.3).

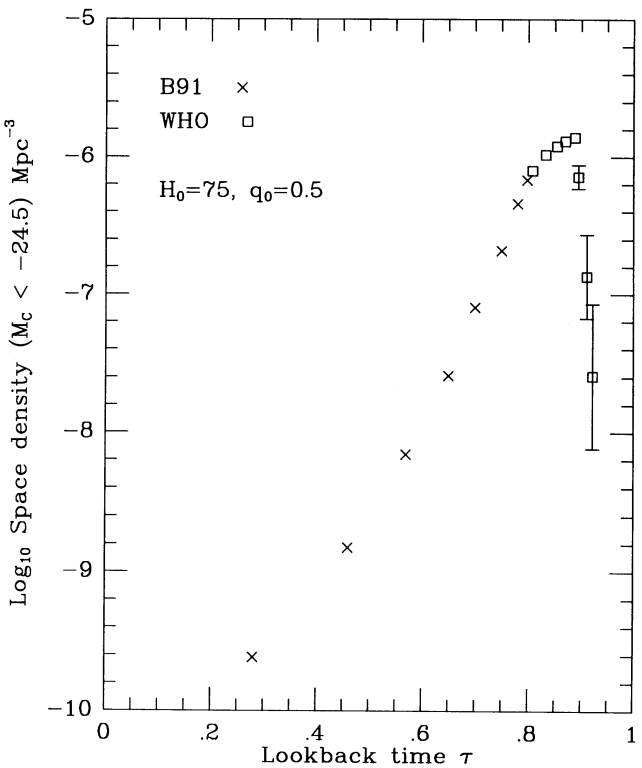

FIG. 8.—Space density of quasars with $M_C < -24.5(q_0 = 0.5)$ as a function of look-back time. The crosses show the results of the Boyle (1991) parameterization for quasars with $z \leq 1.9$. The open squares without error bars are derived from the values in Table 5 for the present sample for the double power-law model. Those with error bars come from the space density at $z = 3.3$ multiplied by the factor exp $[(3.3 - z)k_D]$ and for $k_D = 3.33^{+1.0}_{-1.0}$. The smooth joining of the Boyle points with the present results is an indication of the reliability of the present solution near $z \sim 2$. Note the decline in space density for $\tau > 0.9$.

© American Astronomical Society • Provided by the NASA Astrophysics Data System

1994ApJ...421..412W

4. Predictions for the survey of Irwin et al. (of depth $m_{or} < 19$), based on our solution for the luminosity function, indicate that the space density of bright quasars, $M_C < -27(-26)$, $q_0 = 0.1(0.5)$, declines beyond $z = 3.3$ by a factor similar to our result, and that the space density of such quasars is similar at redshifts ~ 2 and 4.3.

One interpretation of the decline in space density at $z > 3.3$ is that we are seeing back to the epoch of peak formation of high-luminosity quasars, $M_C < -24.5$. For $q_0 = 0.5$, $z = 3.3$ corresponds to a look-back time of 89% of the age of the universe. The data of Figure 8 indicate that the formation occurred in a narrow window of cosmic time, with a FWHM of 10% of the age of the universe. Within the standard model of quasars as the nuclei of active galaxies, this result is telling us about the fueling rate and the mass of the putative nuclear black hole. If quasars are the result of galaxy interactions, then we in turn have information on how galaxies formed and interacted when the universe was a tenth its present age.

However, when we consider that the look-back time corresponds to a path length of 2.4 Gpc, we cannot disregard the possibility that absorbing material along the line of sight, particularly dust in intervening galaxies, causes the apparent decline in space density. This topic has been explored by many (e.g., Wright 1981; Heisler & Ostriker 1988; Fall & Pei 1989); recently Fall & Pei (1993) have presented a detailed treatment of how damped Lyα absorption systems can affect the observed space density. One result that has become clear from such studies is that the optical depth from cosmological absorbers increases steeply with redshift near $z = 3$, close to where we find that the observed space density begins to decrease.

The true situation is more complicated. Fall & Pei note that quantities such as the mean optical depth can be misleading. Magnitude-limited samples select strongly in favor of less obscured quasars; the more obscured ones simply drop out of the sample. They utilize the ratio of true to observed numbers of quasars in a magnitude-limited sample as the most useful quantification of the effects of dust. They present calculations for three models, A (least absorption), B (most likely), C (most absorption), which safely bracket the observational limits for the total H I column density of the absorbers and the dust-to-gas ratio. The results for their model C are a relative decline between $z = 3.3$ and 4 by a factor 3.2(2.8) for $q_0 = 0.0(0.5)$. These values are roughly the same as our 95% confidence limits, so the predicted effects of dust are barely sufficient to explain the amplitude of the observed decline.

Fall & Pei's calculations are based on observations of damped systems in the redshift range $2 < z < 3$, and the predictions for redshifts $z > 3$ are extrapolations. Overall, given the uncertainties in the degree of the decline and in the properties of the absorbers, the hypothesis that the apparent decline in space density at high redshift is caused by dust obscuration continues just to be viable. A comparison of the energy distributions of quasars with and without damped Lyα absorption lines in their spectra, extending the work of Fall & Pei to higher redshifts $z \sim 4$, could test predictions of the dust model.

We gratefully acknowledge the contribution of P. Møller to the computation of the selection functions, through his work on the Lyman line and continuum absorption. S. J. W. acknowledges helpful discussions with M. Schmidt with regard to the comparison of line-flux and continuum-flux limited samples and thanks the Royal Society for support.

APPENDIX A

LYMAN LINE AND CONTINUUM ABSORPTION

The effect on quasar colors of absorption by neutral hydrogen has been computed by creating synthetic spectra of the transmission blueward of the Lyα/N v emission line. This work is based on the study by Møller & Jacobsen (1990), and more details may be found in the article by Møller & Warren (1991). The principles of the modeling are as follows. An imaginary line of sight to a quasar of given redshift intersects absorbers whose properties and location are a particular Poissonian realization of the average distributions for the column density and Doppler parameter as a function of redshift. The transmission spectrum is the product of the transmission spectra of the individual absorbers: these spectra are computed in the manner of Møller & Jakobsen (1990), accounting for line absorption for the first 17 transitions of the Lyman series, and applying continuum absorption below the Lyman limit with the appropriate wavelength dependence of the H I photoionization cross section.

The absorbers were presumed to comprise three populations spanning different ranges of column density, viz., $10^{20} \leq N_{\rm H\,I} < 10^{22}$ cm^{-2} (damped), $10^{17} \leq N_{\rm H\,I} < 10^{20}$ cm^{-2} (Lyman-limit), $10^{12.5} \leq N_{\rm H\,I} < 10^{17}$ cm^{-2} (Lyman-forest). A Doppler parameter $b = 30$ km s^{-1} was assumed for each population. The column density distribution for each was taken to be a power law

$$N(N_{\rm H\,I})dN_{\rm H\,I}dz = C(z)N_{\rm H\,I}^{s}dN_{\rm H\,I}dz\ , \tag{A1}$$

where the normalization evolves with redshift as $C(z) = C(0)(1 + z)^{\gamma}$. The three parameters $C(0)$, s, γ, then, completely specify the column-density distribution for each population, at any redshift. The adopted values of these parameters for the three populations are listed in Table 10 and were selected as described below.

TABLE 10

ABSORPTION-MODEL PARAMETERS

Population	$C(0)$	s	γ
Damped	6.88×10^{13}	−1.73	0.50
Lyman-limit	2.76×10^{9}	−1.60	1.52
Lyman-forest	9.57×10^{8}	−1.60	2.30

© American Astronomical Society • Provided by the NASA Astrophysics Data System

1994ApJ...421..412W

For the damped systems we adopted the results of Lanzetta et al. (1991), for their sample D1 which is limited to column densities $N_{\rm H\,I} > 4 \times 10^{20}$ cm^{-2}. They measured $s = -1.73 \pm 0.29$, and a line density $dN/dz = 0.16$ at an average redshift $z = 2.46$. The evolutionary parameter γ is only very poorly constrained by their data, and we have assumed a value $\gamma = 0.5$. The quoted value of $C(0)$ is then determined from γ, s, and the above value of dN/dz by extrapolating to $z = 0$. Inclusion of the damped systems has only a small influence on the distribution of quasar colors.

Values of γ for the Lyman-limit and Lyman-forest systems are those quoted by Møller (1991). The parameters s and $C(0)$ were determined by comparing mean model transmission spectra against the mean transmission spectrum measured for the 30 quasars in the redshift range $2.75 < z < 3.05$ in the sample of SSB. These quasars were all discovered either in radio surveys or on the basis of emission lines in objective-prism spectra. It is therefore reasonable to suppose that the sample is unbiased with respect to Lyman line and continuum absorption. The median redshift of these quasars is $z = 2.88$, and the column density distribution was assumed to be a single power law at this redshift over the entire range $10^{12.5} < N_{\rm H\,I} < 10^{20}$ cm^{-2}. As shown by Møller & Warren (1991) there is then a unique solution for the slope and normalization of the column density distribution that matches the observed mean transmission spectrum at all wavelengths. The best fit yielded the values of s and $C(0)$ given in Table 10.

Finally, it is now well established that close to the quasar emission redshift $z_{\rm em}$ there is a deficit of lines relative to the number seen at the same observed wavelength in the spectrum of a quasar of higher redshift. This phenomenon has been dubbed the inverse effect (Murdoch et al. 1986) and is believed to indicate a higher degree of ionization of the clouds due to the enhanced ionizing radiation field close to the quasar. This has a significant effect on the inferred unabsorbed Lyα/N v emission-line EWs, and therefore needs to be accounted for if we are to derive the line luminosity function. If the clouds are indeed highly ionized the effect is quite easy to model for unsaturated lines. In this case the absorption line EWs are proportional to the column density, and so the relation between the observed absorption equivalent width EW_a to that which would be seen for the same cloud unaffected by the quasar $\mathrm{EW}_a(0)$ is

$$\mathrm{EW}_a = \mathrm{EW}_a(0)/(1 + Q/B)\,, \tag{A2}$$

where Q is the ionizing flux due to the quasar and B that due to the background. In fact because the column-density distribution slope $s > -2$ the total line absorption is dominated by lines of column density near the transition between the linear (unsaturated) and the logarithmic (saturated) part of the curve of growth. To approximate the inverse effect, therefore, we have supposed the unsaturated case. Murdoch et al. found for the bright quasars in their sample at $z \sim 3$ that $Q = B$ at an interval $\Delta z = 0.044$ from the emission redshift. Since our quasars are some two magnitudes fainter we have adopted an interval $\Delta z = 0.02 \equiv \Delta z_{\rm rest\ frame} = 0.005 \equiv \Delta\lambda_{\rm rest\ frame} = 6.08$ Å. Thus in our adopted model to account for the inverse effect the absorption at a particular wavelength at an interval $\Delta\lambda_{\rm rest\ frame}$ to the blue of the Lyα emission-line center is multiplied by the factor

$$f = 1/[1 + (6.08/\Delta\lambda_{\rm rest\ frame})^2]\,. \tag{A3}$$

For each of 23 redshift intervals $2.2 \le z < 4.5$, $\Delta z = 0.1$, 100 transmission spectra were created. By construction, the effect on quasar colors is accurately modeled near $z = 2.9$, but extrapolation to lower and higher redshifts depends on the correctness of the evolutionary behavior assumed. The acceptability of the model over quasar–rest frame wavelengths from the Lyα/N v emission line down to the Lyman limit has been checked by comparing the average absorption in the synthetic spectra against the average absorption measured in several high-redshift quasars. For this comparison we removed any multicolor-selected quasars from the observational data set. The remaining quasars come from radio or slitless spectroscopy surveys. Although this sample may still not be strictly unbiased with respect to absorption, the range of amount of absorption seen should be representative of the true range.

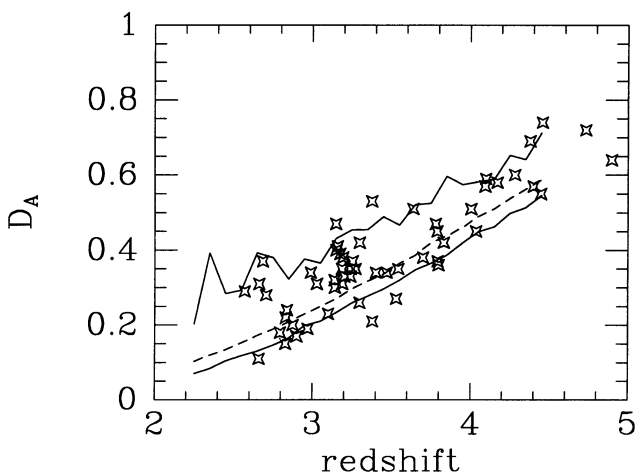

FIG. 9a

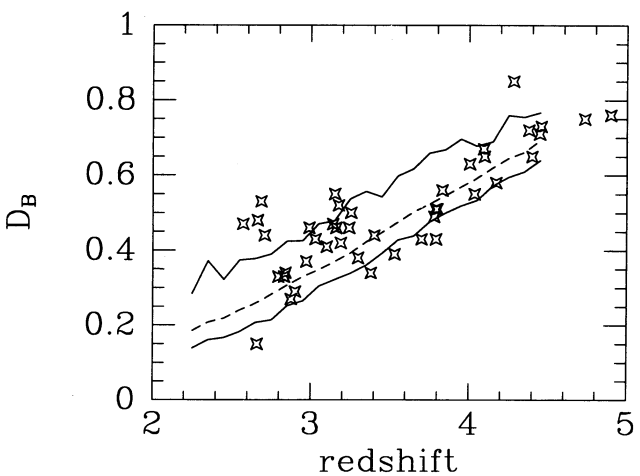

FIG. 9b

FIG. 9.—Comparison between measured line absorption and model, as a function of redshift. Left panel D_A vs. redshift (56 quasars), right panel D_B vs. redshift (43 quasars). The observational data were taken from Schneider, Schmidt, & Gunn (1991a, b) (removing our own multicolor quasars from this data set), SSB, Giallong & Cristiani (1990), and Oke & Korykansky (1982). BAL quasars were removed from these samples, as they are treated differently (Paper II), and where a quasar has been measured more than once we took the most recent value. For the model the median value (*dashed line*) and the 2 σ range (*solid lines*) were established from the measured values of D_A and D_B for 100 synthetic absorption specta at each of 23 redshifts.

© American Astronomical Society • Provided by the NASA Astrophysics Data System

1994ApJ...421..412W

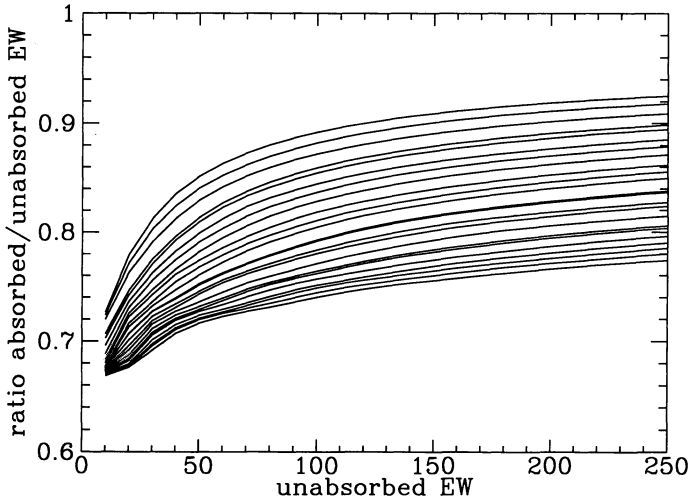

FIG. 10.—Relation between the ratio of the absorbed to unabsorbed EW of the Lyα/N v line as a function of unabsorbed EW. The 23 curves are for different redshifts separated by $\Delta z = 0.1$, starting with the interval $2.2 \leq z < 2.3$, the top curve, through to the interval $4.4 \leq z < 4.5$, the bottom curve. The curves have been used to correct the observed EWs to the unabsorbed values.

The results are shown in Figure 9 where 56 measured values of D_A (the average relative absorption $\lambda\lambda_{\text{rest frame}} = 1050$–$1170$) and 43 measured values of D_B ($\lambda\lambda_{\text{rest frame}} = 920$–$1015$) are plotted against redshift. The dashed line in each plot is the median result for the models, and the solid lines are the 2 σ confidence limits. The accuracy of the measured values of D_A and especially D_B rely on the estimate of the intrinsic continuum level, which is always assumed to be a power law, established by fitting the continuum redward of Lyα/N v and extrapolating. Therefore it is not surprising that a handful of observational points lie outside the model 2 σ limits, and we conclude that the model provides a satisfactory representation of the absorption down to the quasar–rest frame Lyman limit, over the redshift range of interest.

With respect to the continuum absorption the accuracy of the adopted values of γ is unimportant in moving to redshifts lower than the anchor point at $z = 2.9$ since the redshifted Lyman limit lies blueward of the u band for redshifts $z < 2.7$. We found also that the distribution of quasar colors near $z = 4$ was fairly insensitive to the assumed value of γ for the Lyman-limit systems, because the accumulated continuum absorption due to the low column-density Lyman-forest systems is in any case very strong at these redshifts.

In Figure 10 we show the effect of the line absorption on the observed EW of the Lyα/N v line. The curves are the relation between the ratio of the absorbed to unabsorbed line EW as a function of unabsorbed EW, for different redshifts. These curves have been used to correct the measured EWs for the multicolor sample, in order to place the quasars into the appropriate spectral class. Note that the absorbed EW is defined (Paper II) with respect to the continuum fit to the spectrum redward of the line, and extrapolated beneath the line. The correction factors would be very different if, as in the case of the surveys of SSG, the continuum is interpolated between the levels blueward and redward of the line. In such a case, indeed, the ratio of the absorbed to unabsorbed EW could be greater than unity.

APPENDIX B

QUASAR VARIABILITY

B1. VARIABILITY MODEL

To model the effect of variability on quasar colors measured from plates taken at different epochs one needs to know the character of the variability, that is, the power spectrum of the flux variations. Then, by constructing artificial light curves, one can account for the correlations between magnitude variations at the different epochs. We have developed a model for the variability of samples of optically selected quasars that is based on the photometric data of Bònoli et al. (1979) and of Trevese et al. (1989). We have then checked that the predictions of this model are in agreement with the variability data of Netzer & Sheffer (1983) and of Hook et al. (1991). (In this section we compute absolute magnitudes M_B assuming $q_0 = 0.5$, and $H_0 = 50$ km s^{-1} Mpc^{-1}, for consistency with Hook et al.)

The nature of the variability of optically selected quasars may be inferred from the function $\sigma(t)$, which is the time dependence of the rms magnitude difference for a sample of quasars measured at two different epochs. Bònoli et al. (1979) have suggested a relationship of the form $\sigma(t) \propto 1 - e^{-t/\tau}$. We find that a power law $\sigma(t) \propto t^{\sim 1/3}$ provides a slightly better fit to the Bònoli data (their Fig. 7). Furthermore a power-law form for the power spectrum of the magnitude variations $P(\omega) \propto \omega^{\alpha}$, $\alpha = -1.7$, yields $\sigma(t)$ of this shape, and this is the model we have adopted. To reproduce the range of variability seen in quasar samples we have supposed that the distribution of the normalization of the amplitude spectrum $A(\omega) = [P(\omega)]^{1/2} = C \cdot \omega^{\alpha/2}$ is uniform between minimum and maximum values C_{min}, C_{max}. These two parameters together with α specify the model.

© American Astronomical Society • Provided by the NASA Astrophysics Data System

1994ApJ...421..412W

Trevese et al. (1989) have studied the variability of stellar objects in Selected Area 57, using photographic plates from seven different epochs spanning a period of 11 years. We have determined values of $C_{\min}$ and $C_{\max}$ by fitting to the results of their photometry of the quasars found previously in this field by Koo & Kron (1988), selected by color. The comparison was limited to the 21 confirmed quasars $z \leq 2.2$ as this subsample should be largely unbiased with respect to variability. (Our color modeling suggests that this may not be the case for redshifts $z > 2.2$.) Trevese et al. define a variability index σ^* for a quasar which is the rms value of the difference between the magnitude at each epoch and the mean magnitude over the complete time interval sampled. The first four moments of σ^* for the sample of 21 quasars are provided in Table 11, together with the 1 σ errors computed by the bootstrap technique. The parameters $C_{\min}$ and $C_{\max}$ for our model were determined by selecting trial values and constructing light curves for each quasar, computing the moments of σ^*, and comparing against the measured moments. In detail, a light curve over 8192 rest-frame weeks is constructed by selecting random antisymmetric phases, and a random number from a uniform distribution between $C_{\min}$ and $C_{\max}$ for the normalization of the amplitude spectrum. The zero-frequency term of the amplitude spectrum is set to zero. In other words the light curve represents the magnitude *changes* over the 8192 weeks. The amplitude and phase arrays are transformed to Cartesian coordinates, and in taking the inverse Fourier transform we normalize by the factor 1/8192, following convention. To compute the light curve for each quasar as it would have been measured on the plates, due allowance is made for the effects of photometric error and of time dilation by the factor $(1 + z)$. Finally a value of σ^* is computed for each quasar using the procedures listed by Trevese et al. Values of $C_{\min} = 0.55/3.0$, $C_{\max} = 0.55 \times 3.0$, that is, a range of nine of the degree of variability of the quasars, provided a good fit. The expected values for the moments of σ^*, and their errors, for this model, are provided in Table 11. The fact that the errors computed for the model are in good agreement with the bootstrap errors for the data is additional evidence that the model is a good one.

The 21 quasars used in deriving the model have median $M_B \sim -23$, $z \leq 2.2$, and the variability data span 11 years. We have tested the model by comparing against two other samples of different absolute magnitude, redshift, and temporal coverage. First, we used the results of Netzer & Sheffer (1983) which comprise photometry of 64 optically selected quasars at two epochs 31 years apart. These objects were originally identified by their spectra on objective-prism plates, so there should be no bias with respect to variability. We excluded from their list quasars for which the redshifts are uncertain, reducing the sample size to 48. The sample median absolute magnitude is $M_B \sim -27$, and redshifts up to $z = 3.14$ are represented. The first four moments of the absolute values of the magnitude difference $|\Delta m|$ are listed in Table 11. Beneath these the results for the model are provided, calculated as before including the effects of photometric error and of time dilation. The model gives a satisfactory fit despite the substantial differences in absolute magnitude and timespan in comparison with the Trevese et al. data. This suggests that the degree of variability of quasars is not a strong function of absolute magnitude, and that the parameterization of the function $\sigma(t) \propto t^{1/3}$ is an adequate representation of the true form.

In addition we have compared the model to the large sample of Hook et al. (1991). Although this sample is the best in existence in terms of size and redshift coverage, most of the high-redshift quasars $z \geq 2.2$ are in fact our own multicolor-selected objects, and our color simulations show that the degree of variability of each quasar was a factor in determining that it was discovered. The sense of the bias introduced depends on the brightness, the redshift, and the quasar spectral type. For example, variable bright quasars at $z \sim 2.4$ may be lost because of being scattered to a color bluer than our ultraviolet excess cut. On the other hand at redshifts $z \sim 3.7$, at faint magnitudes, only variable objects scattered out of the stellar locus would have been found. As a rule high-variability quasars are lost at bright magnitudes, and low-variability quasars are lost at faint magnitudes.

Hook et al. (private communication) have recently incorporated photometry from two more plates into their database, which now samples seven epochs spanning 16 years. These results were kindly made available to us by I. M. Hook, and in Figure 11 we have plotted their variability statistic σ_v against redshift and absolute magnitude for each of the 317 quasars. The large filled symbols are the median values in bins $\Delta z = 0.6$, $0.3 < z \leq 3.9$, and $\Delta M_B = 1.0$, $-29.0 < M_B \leq -23.0$. For each bin the open square plots the expected value of the median, computed from the model, and the error bars show the 1 σ confidence limits *for the median.* The model lies above the data at bright absolute magnitudes, and this is still true if the sample is limited to redshifts $z < 2.2$, so this discrepancy is unlikely to be due to biases in the sample. It suggests a weak dependence of degree of variability on absolute magnitude. Nevertheless the difference is not very significant, and we consider that our model is satisfactory for establishing the influence of variability on the colors of quasars measured at different epochs.

B2. SENSITIVITY OF THE LUMINOSITY FUNCTION RESULTS TO THE ACCURACY OF THE VARIABILITY MODEL

The results summarized in Table 11 show that the variability model is in good agreement with the observational data. However, the accuracy of the model is limited by the relatively small size of the sample of Trevese et al. We find that the model-quasar magnitude variations could be 30% larger or smaller and still be consistent with the measurements of Trevese at the 2 σ level. Thus if the parameters $C_{\min}$, $C_{\max}$ are reduced (increased) by 30%, the mean value of σ^* for the model for the sample of Treverse et al. goes down (up) by 25%, which is a 2 σ change (the change is smaller than 30% since the photometric errors also contribute to σ^*).

TABLE 11

VARIABILITY RESULTS

Sample	Mean	Sigma	Skewness	Kurtosis
Trevese et al. (σ^*)	0.18 ± 0.02	0.11 ± 0.02	0.89 ± 0.37	-0.12 ± 1.00
Model fit	0.17 ± 0.02	0.09 ± 0.02	0.64 ± 0.39	-0.41 ± 0.90
Netzer & Sheffer ($\lvert\Delta m\rvert$)	0.40 ± 0.05	0.37 ± 0.06	1.43 ± 0.43	2.31 ± 1.77
Model prediction	0.44 ± 0.06	0.39 ± 0.07	1.36 ± 0.50	1.97 ± 2.43

© American Astronomical Society • Provided by the NASA Astrophysics Data System

1994ApJ...421..412W

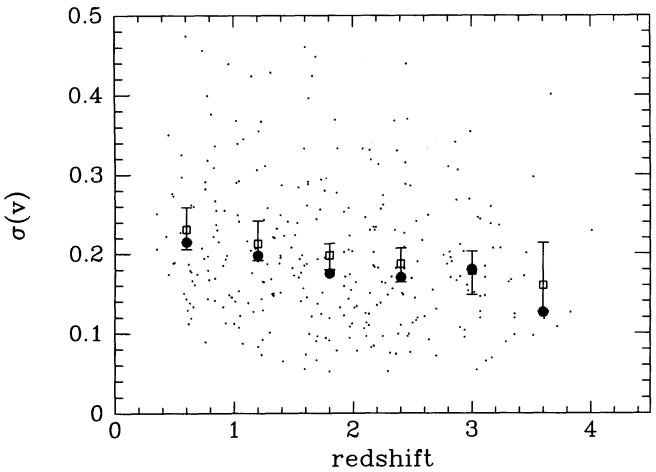

FIG. 11*a*

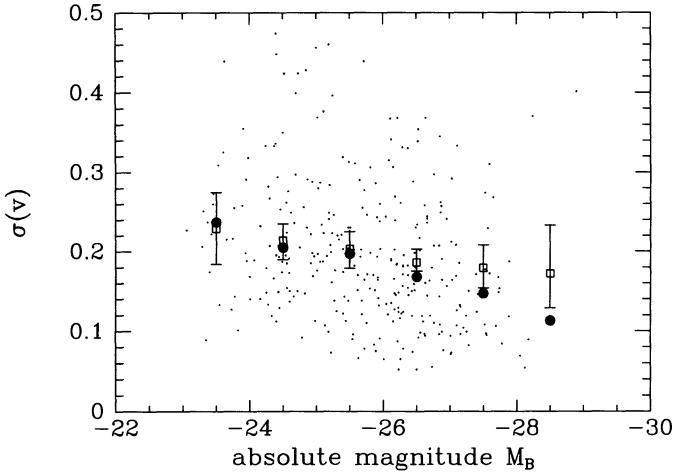

FIG. 11*b*

FIG. 11.—Comparison between the variability of the quasars in the sample of Hook et al. (1991) and the predictions of our model. The variability index $\sigma(v)$ is plotted against redshift (*left*) and absolute magnitude M_B (*right*) from each of the 317 quasars (*small points*). The large filled circles are the median values of $\sigma(v)$ in bins of size $\Delta z = 0.6$, $\Delta M_B = 1.0$. The open squares, with error bars, are the predicted values for the median, based on the model.

Therefore to quantify the sensitivity of the luminosity function results to the accuracy of the variability model we have recomputed the selection functions, scaling the model-quasar magnitude variations by $\pm 30\%$. All other input to the selection-function modeling was left unchanged. With the new selection functions we recomputed the maximum-likelihood model fits for the redshift range $2.0 \leq z < 3.5$ and compared the resulting space densities with the models of Table 5. At bright absolute magnitudes, above the break, the results are virtually unchanged. At fainter absolute magnitudes the largest change at any absolute magnitude, at any redshift, was only 16%. This change is smaller than the 1 σ error on the luminosity function associated with the size of the high-redshift sample (Fig. 5*c*). We conclude that the uncertainty in the variability model does not limit the accuracy of the luminosity function results.

APPENDIX C

LUMINOSITY FUNCTION CALCULATION INPUT DATA

The redshift, apparent magnitude, spectral type, and detection probability of each of the 100 high-redshift quasars used in the calculation of the quasar luminosity function are listed in Table 12. The quasars are taken from three samples:

1. The complete sample of 86 quasars from our multicolor survey in the SGP and F401 fields, referred to as WHO in the table. covering $16.00 \leq m_{or} \leq 20.00$, $2.2 \leq z < 4.5$, effective area 43 deg^2.
2. The three quasars in the survey of Mitchell et al. (1990), referred to as MMB in the table, covering $17.00 \leq m_{or} \leq 18.50$, $3.4 \leq z < 4.1$, effective area 145 deg^2.
3. The brightest 11 quasars in the survey of Osmer & Smith (1980), referred to as OS in the table, covering $16.00 \leq m_{or} \leq 17.30$, $2.2 \leq z < 3.3$, area 340 deg^2.

Below we explain how this table has been drawn up, dealing with each of the three surveys in turn.

WHO sample. The 86 quasars listed comprise the 14 previously known high-redshift quasars in List B (defined in Paper I) in the SGP field, and the 71 new high-redshift quasars in List B from both fields, with the addition of the quasar 0046−282, $z = 3.83$. This list was compiled by reference to Tables 1, 3, and 4 of Paper II, and has been sorted on right ascension. The inclusion of quasar 0046−282 arises because, in addition to candidates in List B in each field we obtained spectra of a number of objects that are red in $m_{bj} - m_{or}$, and blue in $m_{or} - m_i$, looking for quasars of redshift $z \sim 4$. In the SGP we observed all candidates which satisfied simultaneously $m_{bj} - m_{or} > 1.6$ and $m_{bj} - m_{or} > 2.5(m_{or} - m_i) + 0.5m^*_{or} - 8.4$, where m^*_{or} is the larger value of m_{or} and 18.0 (these limits refer to the search photometric system as defined in Paper I). In F401 the criteria were $m_{bj} - m_{or} > 1.6$ and $m_{bj} - m_{or} > 2.5(m_{or} - m_i) + 0.5m^*_{or} - 8.0$. Therefore we may extend the definition of the complete sample to include quasars that satisfy these color criteria. This brings the quasar 0046−282 into the complete sample and increases the selection function probabilities at redshifts near $z = 4$. The combined effect is a reduction in the errors in the determination of the space density at these redshifts.

For 76 of the 86 quasars values are provided in Paper II of the spectral index and EW of the Lyα/N v emission line. We have corrected the equivalent widths for the effect of absorption (Appendix A), and binned the quasars by spectral type, column 4. The spectral type is defined by the combination of spectral index and line equivalent width, as listed in Table 13. For each of these quasars we have compared the measured colors against the distribution of colors for 100 synthetic spectra created for that particular redshift, apparent magnitude, and spectral type. In seven cases, as marked in Table 12, we could obtain agreement only for a different spectral-index bin. In such cases we believe our measured value of α is wrong, and we have changed the spectral type. In a

© American Astronomical Society • Provided by the NASA Astrophysics Data System

1994ApJ...421..412W

TABLE 12

LUMINOSITY FUNCTION CALCULATION INPUT DATA

Sample	Number	z	m_{or}	Spectral Type	p	Sample	Number	z	m_{or}	Spectral Type	p
WHO (SGP)	0039−304	2.21	19.81	5[a]	0.030	WHO (SGP)	0103−263	3.07	19.98	6[a]	0.283
	0040−279	3.23	19.02	1	0.438		0103−301	3.12	19.56	4	0.182
	0040−283	2.33	18.78	6	0.556		0103−290	2.87	17.93	3	0.844
	0041−309	2.83	19.39	5[a]	0.056		0103−294	3.11	19.52	2	0.378
	0041−271	2.79	17.52	5	0.435		0103−260	3.36	18.45	4	0.577
	0042−264	3.29	17.55	5	0.735		0103−292	2.80	18.15	5	0.311
	0042−266	2.98	19.46	2	0.107		0104−275	2.49	18.53	(5)[b]	0.273
	0042−269A	3.33	18.29	5	0.758		0105−278	2.70	18.54	4	0.118
	0042−269B	2.90	18.26	3	0.822		0105−284	2.88	19.25	7	0.035
	0042−276	2.43	18.98	5	0.184						
	0043−296	2.24	18.68	5	0.325	WHO (F401)	2035−344	3.01	19.00	5	0.214
	0043−265	3.44	18.34	4	0.528		2035−261	2.32	18.77	1	0.219
	0043−305	2.39	19.20	(2)[b]	0.270		2038−371	3.00	18.29	1.	0.367
	0043−261	3.11	19.55	5	0.302		2039−375	2.29	19.51	1	0.102
	0044−273	3.16	19.75	3	0.309		2042−366	2.44	19.19	2	0.200
	0046−267	3.52	19.74	3	0.232		2043−331	2.86	19.26	2	0.127
	0046−282	3.83	19.22	5	0.108		2043−347	3.35	18.49	4	0.577
	0047−286	2.99	19.39	5	0.108		2043−338	3.24	18.87	5	0.590
	0047−293	2.41	19.55	(2)[b]	0.142		2043−340	3.10	18.64	5	0.234
	0047−268	3.16	19.67	9	0.320		2043−328	2.69	17.96	4	0.239
	0047−308	2.97	18.00	5	0.278		2045−373	2.86	18.47	5	0.192
	0047−307	3.18	19.08	5	0.388		2048−367	2.26	19.36	(2)[b]	0.156
	0048−309	2.29	19.19	(2)[b]	0.215		2049−362	3.27	19.04	3	0.794
	0048−269	2.32	19.77	2	0.109		2049−375	2.34	18.24	(5)[b]	0.496
	0049−297	2.96	19.06	2	0.230		2049−353	3.04	18.00	3	0.784
	0049−272	2.48	18.70	(5)[b]	0.300		2050−359	3.49	17.81	5	0.762
	0050−283	3.36	19.64	5	0.245		2051−373	2.59	17.19	5	0.505
	0052−290A	2.93	19.99	4	0.077		2051−329	3.06	19.37	2	0.198
	0052−307	2.45	19.67	6[a]	0.185		2054−342	3.03	19.20	8	0.102
	0053−278	3.11	19.95	2	0.298		2054−355	3.31	17.64	5	0.874
	0053−258	2.23	19.64	(5)[b]	0.051		2055−331	2.24	19.30	(2)[b]	0.185
	0053−303	3.07	19.13	2	0.242		2055−361	2.64	18.43	6	0.407
	0053−302	2.44	19.12	9	0.097		2057−366	2.69	17.98	6[a]	0.694
	0053−284	3.62	18.16	6	0.812		2058−333	3.17	18.59	4	0.312
	0054−293	2.96	18.90	6[a]	0.434		2059−360	3.09	18.65	1	0.268
	0054−291	2.53	18.48	8	0.132						
	0055−269	3.66	17.69	3	0.936	MMB	1317−051	3.70	17.7	(5)[b]	0.779
	0055−277	2.43	19.71	3	0.200		1330+011	3.51	18.2	(5)[b]	0.712
	0057−308	2.67	19.27	5	0.056		1426−015	3.42	17.4	(5)[b]	0.727
	0057−282	2.94	18.50	9	0.364						
	0057−274	3.52	18.73	2	0.668	OS	0002−422	2.76	17.1	...	1.0
	0057−302	2.90	18.45	(5)[b]	0.212		0130−403	3.02	17.0	...	1.0
	0057−288	2.43	18.16	4	0.260		0138−381	2.87	17.2	...	1.0
	0058−263	3.05	19.80	2	0.118		0205−379	2.41	16.9	...	1.0
	0058−292	3.07	18.47	1	0.327		0207−398	2.80	17.1	...	1.0
	0059−304B	3.24	19.17	2	0.519		0254−404	2.29	16.9	...	1.0
	0100−280	2.31	19.95	5[a]	0.025		0324−407	3.06	17.2	...	1.0
	0101−304A	4.07	19.51	5	0.221		0.329−385	2.42	16.7	...	1.0
	0101−304B	3.15	17.83	5	0.548		0347−383	3.23	16.9	...	1.0
	0102−285	2.63	18.57	1	0.150		2204−408	3.16	17.1	...	1.0
	0102−301	2.53	19.38	2	0.137		2304−423	2.61	17.2	...	1.0
	0102−293	2.44	18.62	4	0.157						

[a] Spectral type changed (see text).
[b] Spectral type adopted, based on limited or no information (see text).
[c] Magnitudes corrected for Galactic absorption.

number of these cases the error is clearly due to a poor match in flux level between the blue and red halves of our spectra. We assume that the spectral properties of the 76 quasars are representative of the complete sample. In Table 13 the distributions of spectral types for the redshift ranges $2.2 \leq z < 4.5$ and $2.2 \leq z < 3.5$ are summarized.

In order to estimate the detection probability for the 10 quasars lacking complete spectral information we have assumed default values of EW Lyα/N v = 84 Å, and $\alpha = 0.75$, unless the color simulations clearly indicated a different spectral-index bin. The adopted spectral type for each of these quasars is shown in parentheses in the table.

The last column in Table 12 lists the detection probability p. This is the average detection probability for the two fields weighted by their area. The apparent magnitude limit (corrected for Galactic absorption) for F401 is 19.68. Therefore the maximum probability fainter than this is the ratio of the area of the SGP field to the total area, 0.51.

MMB sample. Mitchell et al. (1990) found three bright quasars of redshift $z > 3.4$ in a multicolor survey using plate material similar to our own, although of shorter exposure time. Their selection technique was also similar to our own. The high surface

© American Astronomical Society • Provided by the NASA Astrophysics Data System

1994ApJ...421..412W

TABLE 13

OBSERVED DISTRIBUTION OF SPECTRAL TYPES

Spectral Index	Spectral Type	Equivalent Width Lyα/N v	$2.2 \leq z < 4.5$	$2.2 \leq z \times 3.5$
$0.0 < \alpha < -0.5$.....	1	42	0.092	0.100
	2	84	0.171	0.171
	3	168	0.105	0.086
$-0.5 < \alpha < -1.0$.....	4	42	0.132	0.143
	5	84	0.329	0.329
	6	168	0.092	0.086
$-1.0 < \alpha < -1.5$.....	7	42	0.013	0.014
	8	84	0.026	0.029
	9	168	0.039	0.043

density of stars in our field F401 offsets the benefit from the superior quality of our plates, and we have simply assumed that our selection functions are applicable to their survey.

OS sample. Osmer & Smith (1980) surveyed an area of 340 deg^2 for bright quasars by identifying objects with emission lines in an ocular search of objective-prism plates. While this technique is subjective, it should be very effective at the brightest magnitudes. We have calculated the m_{or} magnitudes that would have been observed for their quasars, and taken a cut at $m_{or} = 17.3$, leaving a sample of 11. The magnitudes were calculated from the continuum magnitude $m_v(1475)$ by assuming a spectral index of $\alpha = -0.75$, and correcting for the effect of emission lines in the *or* passband. The peak in the number counts for the whole survey is near $m = 18.5$, so we assume that the subsample of 11 quasars is complete.

REFERENCES

Avni, Y., & Bahcall, J. N. 1980, ApJ, 235, 694
Barrow, J. D., Bhavsar, S. P., & Sonoda, D. H. 1984, MNRAS, 210, 19P
Bònoli, F., Braccesi, A., Federici, L., Zielli, V., & Formiggini, L. 1979, A&AS, 35, 391
Boyle, B. J. 1991, in Ann. NY Acad. Sci. 647, Texas/ESO-CERN Symposium on Relativistic Astrophysics, Cosmology and Fundamental Physics, ed. J. D. Barrow, L. Mestel, & P. A. Thomas, 14
Boyle, B. J., Fong, R., Shanks, T., & Peterson, B. A. 1990, MNRAS, 243, 1
Boyle, B. J., Shanks, T., & Peterson, B. A. 1988, MNRAS, 235, 935
Fall, S. M., & Pei, Y. C. 1989, ApJ, 337, 7
———. 1993, ApJ, 402, 479
Felten, J. E. 1976, ApJ, 207, 700
Giallongo, E., & Cristiani, S. 1990, MNRAS, 247, 696
Giallongo, E., & Vagnetti, F. 1992, ApJ, 396, 411
Heahnelt, M. G., & Rees, M. J. 1993, MNRAS, 263, 168
Heyes, D. S., & Latham, D. W. 1975, ApJ, 197, 593
Heisler, J., & Ostriker, J. P. 1988, 332, 543
Hewett, P. C., Foltz, C. B., & Chaffee, F. C. 1993, ApJ, 406, L43
Hook, I. M., McMahon, R. G., Boyle, B. J., & Irwin, M. J. 1991, in The Space Distribution of Quasars, ed. D. Crampton (San Francisco: ASP), 67
Irwin, M. J., McMahon, R. G., & Hazard, C. 1991, in The Space Distribution of Quasars, ed. D. Crampton (San Francisco: ASP), 117
Johnson, H. L., Mitchell, R. I., Iriarte, B., & Wisniewski, W. Z. 1966, Commun. Lunar Planet. Lab., 4, 99
Koo, D. C., & Kron, R. G. 1988, ApJ, 325, 92
Lanzetta, K. M., Wolfe, A. M., Turnshek, D. A., Lu, L., McMahon, R. G., & Hazard, C. 1991, ApJS, 77,1
Marshall, H. L., Avni, Y., Tananbaum, H., & Zamorani, G. 1983, ApJ, 269, 35
Mitchell, P. S., Miller, L., & Boyle, B. J. 1990, MNRAS, 244, 1
Møller, P. 1991, in Physical Cosmology, ed. A. Blanchard et al. (Gif-sur-Yvette: Editions Frontières), 527
Møller, P., & Jakobsen, P. 1990, A&A, 228, 299
Møller, P., & Warren, S. J. 1991, in The Space Distribution of Quasars, ed. D. Crampton (San Francisco: ASP), 96
Murdoch, H. S., Hunstead, R. W., Pettini, M., & Blades, J. C. 1986, ApJ, 309, 19
Netzer, H., & Sheffer, Y. 1983, MNRAS, 203, 935
Oke, J. B., & Korykansky, D. G. 1982, ApJ, 255, 11
Osmer, P. S. 1982, ApJ, 253, 28
Osmer, P. S., & Smith, M. G. 1980, ApJS, 42, 333
Peacock, J. A. 1983, MNRAS, 202, 615
Sargent, W. L. W., Steidel, C. C., & Boksenberg, A. 1989, ApJS, 69, 703 (SSB)
Schmidt, M., & Green, R. F. 1983, ApJ, 269, 352
Schmidt, M., Schneider, D. P., & Gunn, J. E. 1986, ApJ, 306, 411
———. 1987, ApJ, 321, L7
———. 1988, in Proceedings of a Workshop on Optical Surveys for Quasars, ed. P. S. Osmer, A. C. Porter, R. F. Green, & C. B. Foltz (San Francisco: ASP), 87
———. 1991, in The Space Distribution of Quasars, ed. D. Crampton (San Francisco: ASP), 109
Schneider, D. P., Schmidt, M., & Gunn, J. E. 1991a, AJ, 101, 2004
———. 1991b, AJ, 102, 837
Trevese, D., Pittella, G., Kron, R. G., Koo, D. C., & Bershady, M. 1989, AJ, 98, 108
Warren, S. J., Hewett, P. C., Irwin, M. J., McMahon, R. G., Bridgeland, M. T., Bunclark, P. S., & Kibblewhite, E. J. 1987, Nature, 325, 131
Warren, S. J., Hewett, P. C., Irwin, M. J., & Osmer, P. S. 1991a, ApJS, 76, 1 (Paper I)
Warren, S. J., Hewett, P. C., & Osmer, P. S. 1991b, ApJS, 76, 23 (Paper II)
———. 1991c, in The Space Distribution of Quasars, ed. D. Crampton (San Francisco: ASP), 139
Wright, E. L. 1981, ApJ, 250, 1

© American Astronomical Society • Provided by the NASA Astrophysics Data System